Fluorophlogopite-bearing and carbonate metamorphosed xenoliths from the Campanian Ignimbrite (Fiano, southern Italy): crystal chemical, geochemical and volcanological insights

M. LACALAMITA[1], G. BALASSONE[2], E. SCHINGARO [1,*], E. MESTO [1], A. MORMONE[3], M. PIOCHI[3], G. VENTRUTI[1], M. JOACHIMSKI[4]

[1]Dipartimento di Scienze della Terra e Geoambientali, Università degli Studi di Bari ALDO MORO, via Orabona 4, I-70125 Bari, Italy

[2]Dipartimento di Scienze della Terra, Università "Federico II", via Mezzocannone 8, I-80134 Napoli, Italy

[3]Istituto Nazione di Geofisica e Vulcanologia, Osservatorio Vesuviano, via Diocleziano 328, I-80124 Napoli, Italy

[4]GeoZentrum Nordbayern, Universität Erlangen-Nürnberg, Erlangen 91054, Germany

* Corresponding author: Prof. E. Schingaro
Tel.: +39-080-5442587, Fax: +39-080-5442591
Dipartimento di Scienze della Terra e Geoambientali
Università degli Studi di Bari
Via Orabona 4, I-70125 Bari, Italy
E-mail: emanuela.schingaro@uniba.it

Mineralogical Society

This is a 'preproof' accepted article for Mineralogical Magazine.
This version may be subject to change during the production process.
10.1180/minmag.2016.080.155

ABSTRACT

Fluorine-, boron-, and magnesium-rich metamorphosed xenoliths occur in the Campanian Ignimbrite (CI) deposits at Fiano (southern Italy), at about 50 km northeast of the sourced volcanic area. These rocks originated from Mesozoic limestones of the Campanian Apennines, embedded in a fluid flow. The studied Fiano xenoliths consist of ten fluorophlogopite-bearing calc-silicate rocks and five carbonate xenoliths, characterized by combining mineralogical analyses with whole rock and stable isotope data. The micaceous xenoliths are composed of abundant idiomorphic fluorophlogopite, widespread fluorite, F-rich chondrodite, fluoborite, diopside, Fe(Mg)-oxides, calcite, humite, K-bearing fluoro-richterite and grossular. Out of the five mica-free xenoliths, two are calcite marbles, containing very subordinate fluorite and hematite, and three are weakly meamorphism carbonates, composed of calcite only. The crystal structure and chemical composition of fluorophlogopite approach those of the end member. The Fiano xenoliths are enriched in trace elements with respect to the primary limestones. Comparison between the REE patterns of the Fiano xenoliths and those of both CI and Somma-Vesuvius marble and carbonate xenoliths shows that the Fiano pattern on the whole both overlaps that of Somma-Vesuvius marble and carbonate xenoliths, and yet reproduces the trend of CI rocks. $\delta^{13}C$ and $\delta^{18}O$ values depict the same trend of depletion in the heavy isotopes observed in the Somma-Vesuvius nodules, related to

This is a 'preproof' accepted article for Mineralogical Magazine.
This version may be subject to change during the production process.
10.1180/minmag.2016.080.155

thermometamorphism. Trace element distribution, paragenesis, stable isotope geochemistry and data modelling point to infiltration of steam enriched in F, B, Mg, As into carbonate rocks at temperature of ca. 300-450°C during the emplacement of the CI.

Keywords: Fiano xenoliths, Campanian Ignimbrite, Southern Italy, fluorophlogopite, crystal chemistry, geochemistry.

Introduction

Fluorine-, boron-, and magnesium-rich metamorphosed xenoliths within the distal Campanian Ignimbrite (CI) deposits (Campania region, southern Italy) have attracted the interest of the scientific community since the nineteenth century for their unusual mineralogy and occurrence. Studies were generally devoted to the crystal chemistry of some of the rare minerals found in these rocks, such as fluoborite (Brisi and Eitel, 1957; Flamini *et al.*, 1979; Cámara and Ottolini, 2000), norbergite (White, 1981) and chondrodite (Balassone *et al.*, 2002). The parental rocks of these xenoliths are Mesozoic sedimentary carbonates of the Campanian Apennines. Carbonate fragments were randomly embedded in the pyroclastic flow during its travel to the surface and emplacement there. Their interactions with hot and volatile-rich ignimbritic flow produced thermal metamorphic effects to varying extent, although far from the source volcanic area (e.g., the Phlegraean Fields; Fig.1).

The distinctive characteristic of these xenoliths the ubiquitous presence of later-formed fluorite and the occurrence of F-B-Mg-bearing mineral phases. They were typically found at Fiano, ca. 20 km northwest of Salerno, and east of the Phlegraean Fields (ca. 50 km) and Somma-Vesuvius (ca. 20 km), both active Campanian volcanoes (Fig. 1). Several quarries (the so-called *Tufare*) at Fiano were intensively exploited in the past for tuffaceous building materials, resulting in the recovery of xenoliths containing F-, B-

and Mg-rich minerals (Carati, 1987). The *Tufare* are currently inactive, because of the decreased demand for grey tuff as a building stone (de Gennaro *et al.,* 2013). Similar xenoliths have been described in the CI exposed in the Caserta province (Scacchi, 1888, 1890; Zambonini, 1919; Carati, 1987), and in tuffs from the Colli Albani volcanic area of the Latium region (the "*Pozzolane nere*" of Corcolle, near Tivoli: Bachechi *et al.,* 1966; Turi, 1969; Masi and Turi, 1972; Caponera *et al.,* 2003).

Although the Fiano xenoliths have received a fair amount of attention for over 100 years (Scacchi 1888, 1890; Zambonini 1919; Masi and Turi 1972; Carati 1987), there has not yet been a thorough study taking advantage of the latest developments in methodology and instrumentation. In this study, xenoliths hosted in CI pyroclastic deposits were investigated using combined mineralogical, geochemical and stable isotope analyses. Our results are compared with data based on studies (Barberi and Leoni, 1980; Del Moro *et al.,* 2001; Gilg *et al.,* 2001; Fulignati *et al.,* 2005) of carbonate xenoliths within the Somma-Vesuvius tephra, which also originated from the same Mesozoic sedimentary carbonates constituting the basement under the volcanoes. The results of this study allow an interpretation of the genetic subaerial environment of the xenoliths and of their peculiar mineral assemblages as well as on the conditions during and following the deposition of the Campanian Ignimbrite.

Occurrence

Volcanological context

The Campania region hosts one of the most active volcanic complexes in Europe. Here, the Phlegraean Fields located near Naples (Fig. 1) represent a large cluster of alkaline volcanic vents, including the eponymous caldera (e.g., Piochi *et al.*, 2015; Vitale and Isaia, 2014). The CI eruption dates to ~ 40 ka based on $^{40}Ar/^{39}Ar$ sanidine geochronology (Fedele *et al.*, 2008). Fallout products from this eruption occur over a wide area (from locations within the Tyrrhenian Sea to the Volga River in Russia and the Black Sea: see Giaccio *et al.*, 2008, and references therein), thus representing an important stratigraphic marker in paleoclimate and archaeological studies (e.g., Fedele *et al.*, 2002; Costa *et al.*, 2012).

The CI juvenile tephra range in composition from trachyte to phono-trachyte (Civetta *et al.*, 1997), are mostly glassy and contain 3 to 10 vol% of dominant sanidine and minor plagioclase, diopside, biotite, magnetite and apatite (Civetta *et al.*, 1997; Pappalardo *et al.*, 2008). Major, trace and Sr-isotope geochemistry suggest that these rocks come from a normally stratified magma chamber with the uppermost phono-trachytic magma layer contaminated by hydrothermal fluids prior to eruption (Civetta *et al.*, 1997). Based on feldspar composition, the pre-eruptive temperature was estimated at 850 ± 40°C, lower than the homogenization temperature of 980°C estimated for melt inclusions within clinopyroxene at a pH_2O of 100-200

MPa (Piochi *et al.*, 2008, and references therein). Based on the variation of the volatile contents in melt inclusions trapped at different pressures, magma degassing during the ascent has been suggested (Marianelli *et al.*, 2006). As a result, the glassy groundmass in the juvenile fragments has low H_2O content (0.3-0.6 wt%) and F and Cl concentrations of ~ 0.26 and 0.78 wt%, respectively (Signorelli *et al.*, 2001; Piochi *et al.*, 2008). The Cl content is in the range of variability found in the glassy matrix and in melt inclusions (from 0.34 to 0.89 wt% in Marianelli *et al.*, 2006). Biotite has F contents between 0.7 and 2.5 wt% and Cl concentrations between 0.04 and 0.14 wt% in pumices (Civetta *et al.*, 1997), but has higher F contents (3.39 - 6.76 wt%) in the syenite nodules in the proximal facies of the CI (i.e. the *Breccia Museo* deposit; Fedele *et al.*, 2006, 2008).

Grey and yellow lithified facies are recognized in the CI. The grey facies is characterized by three lithologies with different textures: a basal part with a typical eutaxitic texture (“*Piperno”*), an intermediate part with weakly collapsed scoriae (pipernoid tuff) and an upper chaotic part (Langella *et al.*, 2013, and references therein). Feldspatization to various degree of the grey facies and zeolitization of the yellow facies have been reported (Cappelletti *et al.*, 2003). The CI exposed in the studied area (Fig. 2) can be related to magmas with a trachyphonolite composition, following Civetta *et al.* (1997). The exposure is mainly represented by the Welded Grey Ignimbrite with a thickness from a few metres to a few tens of metres (Langella *et al.*, 2013),

generally composed of grey ash. It is poorly sorted, massive or showing inverse grading, and does not show any traction-induced sedimentary structure. The lowermost massive part is white to cream in colour, relatively fine-grained, and contains sparse pumice lapilli and rare scoria lapilli toward the top. This part becomes gradually darker and grades upwards into a welded grey zone previously called the Grey Tuff, which is composed of rounded scoria lapilli, inversely graded black scoriae, embedded in an ashy matrix with subordinate xenoliths and crystals. Locally, this welded portion shows columnar jointing. At the top of the Welded Grey Ignimbrite, the degree of welding is minor with equant scoria fragments dispersed in an ashy matrix. Sub-vertical elutriation pipes are locally present at various heights. The Welded Grey Ignimbrite is locally overlaid by the Lithified Yellow Tuff, which is made up of an ashy matrix with rounded lapilli to dispersed blocky pumice clasts. The uppermost incoherent unit consists of coarse pumice clasts within an ashy matrix (Langella *et al.*, 2013). In the Campania region, outcrops of the CI are often found overtopping the limestone mountains at altitudes up 1000 m. They can also be the thickest outcrops in the valleys, as a result of the expanded (and therefore turbulent) pyroclastic current (Fisher et al 1993).

The xenoliths

The F-rich xenoliths within the CI ignimbrite were first described by Scacchi (1890) and Zambonini (1919). The authors recognized many newly formed phases, some of which subsequently discredited, like “nocerite”, “grothine” and “fluosiderite”, synonyms of fluoborite, norbergite and chondrodite, respectively (Brisi and Eitel, 1957; White, 1981; Balassone *et* al., 2002). The Fiano mineral assemblage is mainly represented by halides, F-, Mg- and Ca-bearing silicates, carbonates, and oxides, with subordinate borates, arsenates and vanadates (Table 1). The xenoliths exhibit different dimensions, ranging from few millimetres to several centimeters (Carati, 1987). An exceptional occurrence of a block of 2.3x1.4x0.7 m^3 in dimension was described by Scacchi (1890). According to Carati (1987, and references therein), the xenoliths were initially grouped into “micaceous clasts”, “fluoriferous geodes” and “weakly metamorphosed carbonate rocks”. The micaceous xenoliths (1-35 cm in size) have friable mica-bearing crusts, brown to honey yellow in colour. These rocks were considered as derived from limestone protoliths, metamorphosed to a varying extent, and often characterized by one or more crusts and a nucleus constituted by calcite, as a relict of the primary limestone. Fluorite is widespread and pervasive, fluoborite and chondrodite are also common in the various coatings. The “fluoriferous geodes” represent the final product of the metamorphic process affecting the limestone (Masi and Turi, 1972), and are mostly composed of microcrystalline fluorite and rare calcite. The “weakly

metamorphosed carbonate rocks" have variable dimensions, and can locally show fluorite-rich veinlets and voids and/or rare silicates as thin external coatings.

The fifteen xenoliths studied here come from a private collection (Prof. E. Franco). They were sampled in the late 1980s at the top of the grey tuff at Fiano embedded in the Welded Grey Ignimbrite (Fig. 2), close the so-called quarry "B" of Scacchi (1890). These rocks range from ca. 8 to 14 cm in size, and correspond to micaceous and carbonate xenoliths of the above mentioned literature. As shown in Table 2 and described in more detail below, mica-bearing xenoliths (ten samples) are prevailing over carbonate-dominated mica-free samples (five samples).

Analytical methods

The Fiano xenoliths were characterized mineralogically and petrographically by combining polarizing optical microscopy, X-ray powder diffraction (XRPD) and scanning electron microscopy equipped with an energy-dispersive spectrometer (SEM-EDS). XRPD was conducted using a Seifert-GE diffractometer ID 3003 (Dipartimento di Scienze della Terra, dell'Ambiente e delle Risorse, University of Naples, Italy). Intensity profiles were collected in the 2θ range of 3-80° using Ni-filtered CuKα radiation (λ = 1.5406 Å) at 40 kV and 30 mA, with a step size 0.02°, at a scanning time of 10 s/step. The diffraction patterns were processed using the RayfleX

software package. A minor set of measurements were performed by using a X'Pert Powder diffractometer by PANalytical (Istituto Nazionale di Geofisica e Vulcanologia Osservatorio Vesuviano, Naples, Italy), with a high speed PIXcel detector, Ni-filtered CuKα radiation (λ = 1.5406 Å), at 40 kV and 40 mA in the 3-70° 2θ range, with 0.02º steps at 8 s/step. Diffraction patterns were processed and interpreted using the PANalytical B.V. software HIGHScore Plus version 3.0e. SEM examination was carried out using a JEOL JSM 5310 instrument at Dipartimento di Scienze della Terra, dell'Ambiente e delle Risorse, University of Naples, Italy. Element mapping in backscattered electron mode (BSE) and EDS microanalyses were obtained with an INCA X-stream pulse processor and the 4.08 version Inca software (Oxford Instruments detector), interfaced with the JEOL JSM 5310. The following reference standards were used: albite (Si, Al, Na), orthoclase (K), wollastonite (Ca), diopside (Mg), almandine (Fe), rutile (Ti), barite (Ba), strontianite (Sr), metallic chromium (Cr), rhodonite (Mn), pyrite (S), sphalerite (Zn), galena (Pb), fluorite (F), apatite (P), sylvite (Cl), Smithsonian phosphates (La, Ce, Nd, Sm, Y), gallium arsenide (As) and metallic vanadium (V). Analytical errors are 1% relative for major elements and 3% relative for minor elements.

Ten xenoliths, including seven micaceous and three carbonate ones, were selected for whole-rock chemistry, carried out at Bureau Laboratories Ltd. (Vancouver, Canada). Major elements were analysed by X-ray fluorescence

248 (XRF) and inductively coupled plasma emission spectrometry (ICP-ES),
249 using $LiBO_2/Li_2B_4O_7$ fusion. Minor and trace elements were determined by
250 inductively coupled plasma-mass spectrometry (ICP-MS), using a four-acid
251 (HNO_3-$HClO_4$-HF-HCl) digestion. The uncertainty is less than 3% for
252 major/minor oxides, less than 5-10% for trace elements. Loss on ignition
253 (LOI) was calculated by weight loss after ignition at 1000°C.

254 Stable carbon and oxygen isotope analyses were carried out at the
255 University of Erlangen-Nürnberg (Germany) on nine selected calcite-
256 bearing samples (both carbonate and micaceous xenoliths). Carbonate
257 powders (checked for impurities by powder diffraction) were reacted with
258 phosphoric acid at 70 °C using a GasBench II connected to a Thermo
259 Finnigan Five Plus mass spectrometer. Carbon and oxygen isotope values
260 are reported in per mil relative to Vienna Pee Dee Belemnite (VPDB) and
261 Vienna Standard Mean Ocean Water (VSMOW), by assigning $\delta^{13}C$ and
262 $\delta^{18}O$ values of +1.95 and -2.20‰ VPDB to NIST reference material NBS19
263 (limestone), and -46.6 and -26.7‰ VPDB to LSVEC (Li_2CO_3).
264 Reproducibility was checked by replicate analyses of laboratory standards
265 and was ±0.07‰ (1σ) for both carbon and oxygen isotope analyses.

266 Six mica single crystals were selected from three micaceous xenoliths for
267 single crystal X-ray diffraction (SCXRD) analyses. The same crystals were
268 embedded in epoxy resin and polished to perform electron microprobe
269 (EMP) measurements. A JEOL JXA-8200 electron microprobe

(Dipartimento di Scienze della Terra, University of Milan, Italy) operating at 15 kV accelerating voltage, 5 nA sample current on brass, ~ 1 μm spot size and 40 s counting time was used. F, Na, K, Ba, Ca, Cl, Ti, Cr, Mn, Ni, Sr, Zn and Zr contents were analyzed by wavelength dispersive spectrometry whereas Si, Al, Mg and Fe by energy dispersive spectrometry. The used standards were: grossular (Si-Al), forsterite (Mg), omphacite (Na), ilmenite (Ti), rhodonite (Mn), K-feldspar (K), metallic Cr (Cr), fayalite (Fe), wollastonite (Ca), sanbornite (Ba), apatite (F), celestine (Sr), nickeline (Ni), scapolite (Cl), zincian rhodonite (Zn, with ZnO content 7.22 wt%), zircon (Zr). Fluorine was analyzed following the procedure described in Balassone *et al.* (2013). A Phi-Rho-Z routine as implemented in the JEOL suite of programs allowed the conversion from X-ray counts to oxide weight percentages (wt%). Relative uncertainty on the analytical measurements was 1% for major elements and 4% for minor elements. Cr, Sr, Ni, Zr and Ba were all measured but were found below the detection limits (0.04 wt% for Cr, Ni, Zr; 0.09 wt% Ba, Zn, Sr; 0.01 wt% for Ca, Cl).

SCXRD data were collected by means of a Bruker AXS X8 APEXII automated diffractometer (Dipartimento di Scienze della Terra e Geoambientali, University of Bari, Italy) equipped with a CCD detector and graphite-monochromatized MoKα radiation (λ = 0.71073 Å). The instrument operated at 50 kV, 30 mA and 40 mm crystal-to-detector distance. The collection strategy was optimized by the Apex program suite

by combining several ω and φ rotation scans (scan width 1.0°/frame, exposure time 10 s/frame) and recording the whole Ewald sphere (±*h*, ±*k*, ±*l*) up to θ ~ 40°. The SAINT package (Bruker, 2007) was used for the integration of the intensities of reflections and for the correction of Lorentz-polarization. The SADABS software (Bruker, 2009) was employed for the absorption correction. Structure refinements were carried out using the CRYSTALS software (Betteridge *et al.*, 2003). The refined parameters were: scale factors, atomic positions, cation occupancies and anisotropic displacement parameters.

Results

Mineral chemistry, major and trace element geochemistry

The micaceous metamorphosed xenoliths (see Table 2) locally shows a geode-like structure and/or zones composed of different mineral assemblages. Their honey-brown parts are rich in idiomorphic mica crystals, which correspond to fluorophlogopite (see the section below for details). Fluorite is widespread and F-rich chondrodite typically forms deep-red crusts. Fluoborite occurs as tiny needles and is fairly common in some xenoliths (Fig. 3*a*, *b*). Other phases detected in small amounts by combined XRPD and EDS analyses are yellow diopside, Fe(Mg)-oxides (magnetite, magnesioferrite and hematite), calcite, humite, K-bearing fluoro-richterite

313 and grossular. Overall they can be classified as calc-silicate rocks (Rosen et
314 al., 2007).

315 The carbonate metamorphosed xenoliths TF11 and TF15, respectively
316 (Table 2) are mainly composed of calcite, with sporadic vuggy fluorite and
317 hematite. They are friable and have saccharoidal texture, hence they can be
318 classified as marbles (Rosen et al., 2007). The three mica-free samples TF8,
319 TF14 and TF16 (Table 2) are compact rocks composed only of calcite and
320 appear to be less affected by thermal methamorphism; accordingly they are
321 here referred to as weakly metamorphosed carbonates.

322 SEM-BSE images of selected micaceous xenoliths show that fluorite is
323 ubiquitous, and at least two generations can be observed. It is found in
324 crusts, vugs or fracture fillings (Figs. 4*a*-*d*). Sometimes fluorite also occurs
325 as a kind of graphic-like intergrowth in fluoborite (Figs. 4*e* and 4*f*).
326 Fluorophlogopite always has euhedral habit, reaching several millimeters in
327 size. Among other silicates, diospide, chondrodite, grossular and humite
328 generally occur as anhedral crystals and/or aggregates (Fig. 4*g*). K-bearing
329 fluoro-richterite and magnesioferrite are very rare and have not been
330 reported before in the Fiano samples. Other accessory phases are magnetite
331 and hematite (Fig. 4*h*). The mineralogical assemblage in the Fiano xenoliths
332 (Table 2) differs from the mineralogy of Ca-poor ejecta, skarns and marble
333 from the Vesuvius deposits (Barberi and Leoni, 1980; Del Moro *et al.*,
334 2001; Gilg *et al.*, 2001; Fulignati *et al.*, 2005). Specifically, spinel and

335 brucite do not occur in our samples whereas B-bearing minerals are not
336 reported from the Vesuvian ejecta.
337 The results of EDS chemical analyses of the Fiano minerals are reported in
338 Table 3. Among silicates, chondrodite and humite are represented by F-rich
339 varieties (as also reported by Balassone *et al.*, 2002). Following Hawthorne
340 et al. (2012), the Fiano amphibole can be ascribed to a sodic-calcic variety,
341 and in particular to K-bearing fluoro-richterite, with K = 0.25 atoms per
342 formula unit (a.p.f.u.). Compared to potassic-fluoro-richterite from Somma-
343 Vesuvius xenoliths (K equal to 0.67 a.p.f.u., Della Ventura *et al.*, 1992), it
344 shows higher F content (~ 2 vs. 1.27 a.p.f.u. in Somma-Vesuvius
345 amphibole). Very low contents of Mg (0.03 a.p.f.u) and Mn (0.004 a.p.f.u)
346 are found in calcite (Table 3). Fluoborite is close to the end-member
347 $Mg_3(BO_3)F$, with CaO content just above detection limit (0.03 wt. %) and
348 FeO below detection limit (Table 3). High amounts of F (24.33 wt%, Table
349 3) can be related to the low amount of OH in its composition. Fluorite
350 shows an amount of Mg of 0.12 wt.% ("sellaite" content 0.4%). Hematite
351 shows 2.91 wt.% Al_2O_3 (corundum content 4.3%). Different contents of
352 Al_2O_3 were found in magnesioferrite (4.34 wt.%) and magnetite (0.99 wt%);
353 magnesioferrite shows an amount of 4.08 wt.% MnO (in terms of end
354 member composition magnetite 0.50 spinel 7.39 hercynite 0.05 galaxite 0.95
355 magnesioferrite 80.73 jacobsite 10.38), and magnetite shows 0.73 wt%

356 MgO, 0.45 MnO wt.% and 0.21 wt.% CaO (magnetite 92.2 spinel 0.10
357 hercynite 2.11 galaxite 0.04 magnesioferrite 4.11 jacobsite 1.44).
358 Whole rock chemistry (Table 4) shows that Fiano xenoliths are depleted
359 in silica and rich in CaO and MgO, particularly when compared to the
360 Phlegraean magmas (e.g., Piochi et al., 2005; Arienzo et al., 2011;
361 Tomlinson et al., 2012 and references therein). The carbonate xenoliths, as
362 sample TF8, are obviously richest in CaO and most depleted in alkaline
363 elements. The MnO and P_2O_5 concentrations show a large variation (from
364 0.21 to 0.76 wt% and from 0.01 to 0.60 wt%, respectively, see Table 4).
365 Trace elements contents are lower (i.e., REE, HFSE) or comparable (i.e., Cs,
366 Rb, Ba, Th, U, K, Nb, Pb, Sr) to those reported for the CI (Civetta *et al.*,
367 1997; Polacci *et al.*, 2003; Marianelli *et al.*, 2006; Piochi *et al.*, 2008;
368 Tomlinson *et al.*, 2012). The main difference concerns B and As contents
369 ranging up to several thousand ppm in all samples, except for carbonate
370 xenoliths TF8, TF11 and TF15. The high amount of B (7713 ppm on
371 average) in micacaeous xenoliths is obviously related to fluoborite, whereas
372 As contents (2712 ppm on average) might be due to traces of hörnesite
373 (already found at Fiano), even though this mineral was not detected, at least
374 in the fractions analysed by XRD and EDS, likely due to the intrinsic
375 heterogeneities of the samples. However, the presence of other As-bearing
376 minerals cannot be excluded. As shown in Fig. 5, the REE pattern of the
377 studied Fiano xenoliths is characterized by fractionated light rare earth

elements (LREE), negative Eu anomaly, and unfractionated heavy rare earth elements (HREE). Note also that the carbonate xenoliths (yellow symbols in Fig. 5) are slightly depleted in both LREE and HREE compared to the micaceous ones (red symbols), except for Tm. In addition, the REE pattern of the studied Fiano xenoliths parallels the trend of the Campanian Ignimbrite (blue and green symbols) but are displaced by an order of magnitude to lower REE contents. LREE for the Fiano samples overlaps the average of the Somma-Vesuvius marbles and carbonates (peach-coloured band), but the HREE are less fractionated, so that Dy and heavier REE are present in greater amounts in the Fiano samples than the average for the Somma Vesuvius marbles and carbonates, plausibly a result of the peculiar mineral assemblage. If compared to rocks of Somma-Vesuvius, the studied xenoliths are richer in selected major and trace elements, such as silica and Cs, Ba, K, Pb, Rb. Also, xenolith TF9 shows the highest Pb content.

Stable isotope geochemistry

The stable isotope data of calcite from both micaceous and carbonate xenoliths are presented in Table 5. The $\delta^{13}C$ and $\delta^{18}O$ values range from -5.2 to 0.0‰ VPDB and 15.7 to 27.1‰ VSMOW, respectively (Table 5). Carbon and oxygen in the weakly metamorphosed carbonate xenoliths TF14 and TF16 are slightly heavier ($\delta^{13}C$ -0.07 and 0.04‰ VPDB; $\delta^{18}O$ 26.5 and 24.6‰ VSMOW) compared to the other carbonate xenoliths. Sample TF8,

400 another weakly metamorphosed xenolith, also shows heavier $\delta^{18}O$ value
401 (27.1‰ VSMOW) but a lighter $\delta^{13}C$ (-1.60‰ VPDB) value compared to
402 samples TF14 and TF16. All these values are closer to the isotope values of
403 unmetamorphosed Triassic marine carbonates of the Campanian platform
404 (average $\delta^{18}O$ values = 30‰ VSMOW; average $\delta^{13}C$ = 0.79‰ VPDB;
405 Iannace, 1991) with respect to the other Fiano samples (Fig. 6). The isotope
406 values measured for the Fiano xenoliths overlap those of calcites from
407 thermal metamorphic xenoliths (i.e. marbles and skarns) from Somma-
408 Vesuvius (Gilg *et al.*, 2001). Our values also show a partial correspondence
409 with oxygen and carbon isotope data of the Fiano samples measured by
410 Masi and Turi (1972). However, these authors also report $\delta^{13}C$ values
411 considerably lower than those in this study. As on similar samples from
412 Alban Hills (Turi, 1969), the low to very low $\delta^{13}C$ values (<-15‰)
413 probably result from the complex interaction with meteoric waters
414 (recognized for the external part of nodules plotted in the “weathering” field
415 of Fig. 6) and from multiple and superimposed decarbonation processes and
416 isotope exchange reactions with hydrothermal fluids, as discussed below.
417 Moreover, the Fiano $\delta^{18}O$ are much higher than values (8-8.5‰) known for
418 the CI juvenile products (whole rock and feldspar; Taylor et al., 1979)
419 (shaded box in Fig. 6).
420
421

Crystal chemistry of fluorophlogopite

EMP data indicate close similarities among micas from xenoliths TF2, TF7 and TF10 (Table 6). The studied crystals contain ~ 43.7 wt% SiO_2, ~ 11.1 wt% Al_2O_3, ~ 27.2 wt% MgO, ~ 2.1 wt% FeO and ~ 8.8 wt% F. These contents are essentially the same found in the Vesuvius fluorophlogopite from the 1872 eruptions (Balassone *et al.*, 2013), i.e. those of near end-member F species with high Mg and negligible Al in the octahedral sites. Cs is detected in whole rock analysis (up to 65.7 ppm, see Table 4) but was not searched for in micas. However, even if it were completely partitioned into the mica, its content would be < 0.001 a.p.f.u., negligible from crystal chemical viewpoint.

The results of the structure refinements (see the values of the R_1, wR_2, $\Delta\rho_{min}/\Delta\rho_{max}$ and Goof in Table 7), carried out in the expected *C2/m* space group for polytype 1*M* indicate good data and crystal quality. Lattice parameters (on average *a* ~ 5.30, *b* ~ 9.19, *c* ~ 10.13 Å, β ~ 100.08°, Table 7), structure data (supplementary Table S1), mean bond length distances (<T-O> ~ 1.65, <M-O> ~ 2.06, <K-O> ~ 3.13 Å, supplementary Table S2) and polyhedral distortional parameters (supplementary Table S3) are very similar for all the analysed crystals, confirming the substantial chemical and structural homogeneity, already established on the basis of EMP data. The studied crystals are geometrically "homo-octahedral" (i.e., <M1-O> equals to <M2-O> distances within three standard deviations, Weiss *et al.*, 1992).

444 This geometrical feature is consistent with a disordered cation distribution at
445 octahedral sites. A comparison between the mean atomic numbers of cation
446 sites as determined by structure refinement (X-ref) and those calculated
447 from the chemical molar fractions and atomic radii in Shannon (1976) is
448 reported in the supplementary Table S4. The combination of EMP and
449 SCXRD data led to the structural formulae given in Table 8. They were
450 calculated following the procedure described in Ottolini *et al.* (2012) and
451 Schingaro *et al.* (2013). Note that the formulae of the studied samples are
452 similar to those of the Vesuvius fluorophlogopite from the 1872 eruptions
453 (Balassone *et al.,* 2013), apart from a small tetraferriphlogopite component
454 and a greater variability in $^{VI}Fe^{3+}$ content. These data show that the Fiano
455 micas are fluorophlogopite with minor tetraferriphlogopite component.
456 Al,Fe^{3+}-vacancy [$3\,^{VI}M^{2+} \leftrightarrow 2\,^{VI}M^{3+} + {}^{VI}[]$] and $^{XII}K^{+} + {}^{IV}Al^{3+} \leftrightarrow {}^{IV}Si^{4+} +$
457 $^{XII}[]$substitutions also occur. The structural effects of $OH^{-} \rightarrow F^{-}$ substitution
458 in micas were recently reviewed by Balassone *et al.* (2013).
459 Fluorophlogopite is interesting in showing structural distortions mainly
460 along the direction close to the K-O4 bond with a consequent shrinkage of
461 *c*-cell parameter, K-O4 distance, Δ_{K-O} (i.e., difference between $<K\text{-}O>_{outer}$ and
462 $<K\text{-}O>_{inner}$ distances) and interlayer thickness (t_{int} parameter). The values of
463 these parameters for samples TF2, TF7 and TF10 match very well to those
464 determined for other fluorophlogopite samples (e.g., compare Table S3 with
465 Supplemental Data Table 3 in Balassone *et al.,* 2013). Incorporation of

fluorine is also accompanied by reduction of the ditrigonalization of the T sheet and, therefore, by decrease of the in-plane rotation angle (α). This also holds for the Fiano micas that exhibit α values in the range 6-6.40°. Consequently, the studied micas plot very close to end-member fluorophlogopite (Fig. 7) whereas, according to Schingaro *et al.* (2011), very low values of the α correspond to micas affected by extensive $OH^- \rightarrow F^-$ and by significant de-hydrogenation.

Discussion

Mineral association and genetic conditions

The natural variability of fluorine concentration in mica, ideally from 0 to 2 fluorine a.p.f.u., is broadly reflected in the variation of the α distortional parameter from 4 to 11°. In Fig. 7 some F amount corresponds to a very large difference in α. This parameter, as well as all the other crystal chemical features of the studied mica from the TF2, TF7 and TF10 xenoliths, closely approach those of the end-member fluorophlogopite in Gianfagna *et al.* (2007) and Balassone *et al.* (2013), in spite of their different parageneses. Specifically, fluorophlogopite in benmoreitic lava at Biancavilla (Catania, Mount Etna, Sicily) is associated with fluoro-edenite, alkali-feldspars, clino- and ortho-pyroxenes, fluorapatite, hematite, and pseudobrookite. The genesis of this mineral assemblage was ascribed to F- and Cl-rich fluids that have locally metasomatized the benmoreite (Gianfagna *et al.*, 2007).

Fluorophlogopite in xenoliths from Vesuvius AD 1872 eruption (Balassone *et al.,* 2013), instead, was found in association with anhydrous osumilite, sodalite and gypsum. It was hypothesized that the xenoliths formed in a high-temperature (> 700°C) low pressure (<1 kbar) environment from a magma body-sourced volatile component characterized by high concentration of F, and minor concentration of Cl and S.

Although fluorophlogopite is found in diverse mineral assemblages (Gianfagna *et al.,* 2007; Balassone *et al.,* 2013; Scordari *et al.,* 2013; Schingaro *et al.,* 2014), it invariably indicates the presence of significant volatile content in the system. In the case of study, fluorophlogopite from the micaceous xenoliths is associated mainly with fluorite, F-rich chondrodite and fluoborite, and subordinately to diopside, magnetite, magnesioferrite, hematite, calcite, humite, K-bearing fluoro-richterite and grossular, which define a rare and peculiar F (Mg)-rich mineral assemblage. It can be observed that:

1) fluoborite is a relatively rare borate mineral only described in magnesian skarns wordwilde (see Marincea, 2000 and review therein) in association with chondrodite, norbergite and fluorite;

2) humite group minerals occur in some metamorphosed silica-deficient dolostones and limestones (Mg hornfelses and skarns) together with other species, such as diopside, tremolite and spinel (Tell, 1974);

3) K-bearing fluoro-richterite rarely occurs in metamorphic environments; exceptions are, for instance, the thermo-metamorphic ejecta from Somma-Vesuvius volcano, Italy (Della Ventura *et al.,* 1992), and the amphibole-diopside metacherts in marble from Bufa del Diente, Mexico (Heinrich, 1994).

According to Marincea (2000), crystallization of fluorophlogopite and fluoborite requires a substantial activity of fluorine in the boron-bearing metasomatic fluids. Experimentally, "fluoborite" is stable at a temperature of 380÷450°C (Tell, 1974). This is consistent with data on humite that crystallizes from fluorine reactions in silica deficient dolomite between 300 and 560°C, in the pressure range from 700 to 2000 bars (Tell, 1974). This is also in agreement with the temperatures <500-600°C at pressure < 1 kbar which are involved in the occurrence of the K-bearing fluoro-richterite in the metamorphic rocks. Specifically, these conditions were suggested by the breakdown of dolomite *via* the reaction dolomite + SiO_2 = diopside + CO_2 (Della Ventura *et al.,* 1992) in the case of the Somma Vesuvius ejecta.

The potassic-fluoro-richterites from metacherts of Mexico were considered to be formed by the reaction of early diopside formed by contact-metamorphism with pervasive hypersaline brines of magmatic origin (Heinrich, 1994). The Fiano K-bearing fluoro-richterite have likewise formed in the presence of similar F-Na-K(Ca)-rich and Cl-free metasomatic brines at similar temperatures (ca. 500 °C), even if at lower P conditions.

We have observed diopside grains enclosed in K-bearing fluoro-richterite; this evidence might also lead to infer amphibole formation at the expense of clinopyroxene, implying infiltration of metasomatic brines after peak metamorphism (Heinrich, 1994).

The halogen content of fluorophlogopite can be used to evaluate the relative fugacities of H_2O and HF in the fluids using the procedure in Cesare *et al.* (2003). For this calculation the value of the exchange temperature is required. The peak value of biotite crystallization should not be used because the halogen and hydrogen contents of mica may not be primary (Cesare *et al.* 2003), as also discussed above. However, considering our mineral assemblage and the discussion above we calculated the log ($f$$H_2O$)/($f$HF), ($f$$H_2O$)/($f$HCl) and ($f$HF)/($f$HCl) both at 300° and 500°C. The obtained values were 4.1, 4.9 and -1.3 at 300°C and 3.1, 3.7 and -0.9 at 500°C, in both cases indicating that the role of water overwhelms that of other volatiles. Trace element and stable isotope geochemistry support the previous considerations and provide additional geochemical clues pointing to metasomatism for the Fiano xenoliths.

In particular, the REE pattern of the Fiano samples are similar to Somma-Vesuvius metamorphosed and unmetamorphosed carbonate ejecta. However, the enrichment of B, As, Se, Hg in the studied Fiano xenoliths (Table 4) compared to the carbonates and marbles of Somma-Vesuvius is consistent with the easy mobilization of B during prograde metamorphism (Leeman *et*

553 *al.*, 1992). This is also supported by the observation that the samples with
554 lower $\delta^{18}O$ values (e.g. TF5 and TF9 in Fig. 6), i.e., far from the
555 sedimentary protolith, are rich in B and As (Table 4).

556 In addition, the carbon and oxygen isotopes of the Fiano xenoliths
557 indicate a depletion trend of ^{13}C and ^{18}O as similarly observed in the
558 Somma-Vesuvius nodules (see Fig. 6), with the lower values being related
559 to metamorphism at a host-rock magma interface (Gilg *et al.*, 2001).
560 Multistage fractionation processes, which were evident in the very light
561 carbon isotope ratios reported for the Fiano carbonate xenoliths by Masi
562 and Turi (1972), are not apparent in this study.

563 Fig. 8 shows both the covariation in C and O isotopes as well as the
564 expected equilibrium values based on calcite-fluid interaction (Zheng, 1990;
565 Zheng and Hoefs, 1993) and decarbonation processes (Bowman, 1998) at
566 different temperatures, based on mineralogy. The distribution of the isotope
567 values can be related to the interaction of a hydrothermal fluid dominated by
568 HCO_3^- with the carbonate deposits at 100-350°C. This is consistent with
569 high values of the relative fugacity of H_2O calculated from the
570 fluorophlogopite composition of the studied xenoliths (see above). The end-
571 member used for hydrothermal fluids has typically an isotope composition
572 of $\delta^{13}C$ = -13‰ VPDB and $\delta^{18}O$ = 8‰ VSMOW (Zheng and Hoefs, 1993).
573 In addition, a temperature of ca. 300°C required for the isotopic shift is in
574 agreement with the stability conditions of the newly formed

fluorophlogopite. On the contrary, the isotope ratios cannot be explained by the interaction of a magmatic fluid ($\delta^{13}C$ = 0‰ VPDB and $\delta^{18}O$ = 10‰ VSMOW) with the Mesozoic sedimentary carbonate (see "exchange at 750°C" in Fig. 8), as modelled by Fulignati *et al.* (2005). Moreover, decarbonation at 300°C or 500°C cannot explain the observed variation in $\delta^{18}O$ of up to about >-5‰, although this process is in agreement with the lighter isotope values of the Fiano carbonates that were reported by Masi and Turi (1972). Assuming a Rayleigh decarbonation process (Fig. 9), we plotted the carbon and oxygen isotope fractionation between calcite and fluid, $10^3 \ln\alpha$, where $\alpha=(1000+\delta^{13}C)_{calcite}/(1000+\delta^{13}C)_{fluid}$ or $(1000+\delta^{18}O)_{calcite}/(1000+\delta^{18}O)_{fluid}$, based on the measured isotope values (final calcites) relative to the fraction F of carbon or oxygen left in primary calcite (Mesozoic carbonate). Only the reasonable ranges (Bottinga, 1968) of calculated $10^3 \ln\alpha$ values are displayed in Fig. 9. Considering both modelling and the upper oxygen limit for carbonate (F > 0.6; Bowman, 1998), we suggest that decarbonation at around 450°, as derived (see above) by stability temperature for fluoroborite and phlogopite, likely affected the weakly metasomatized Fiano xenoliths (TF8, TF14 and TF16 samples). Moreover, following Bowman (1998), the calculated $10^3 \ln\alpha$ and F values indicate conditions intermediate between "silicatic" disequilibrium and "silica-absent" decarbonation. Therefore, the scatter in Fig. 8 can be also partially derived from an initial decarbonation process prior to the main

hydrothermal alteration of the primary carbonates, within the pyroclastic flow.

Volcanological implications

The CI pyroclastic flow emplaced at Fiano had a temperature range of 300-500°C and underwent hydrothermal processes during its cooling, as registered from the mineralogy and isotope composition of the embedded xenoliths. The intense lithification of the ignimbrite (Cappelletti *et al.*, 2003) and the remnant magnetic susceptibility (e.g., Ort *et al.*, 1999) indicate temperatures of ca. 400° C during the CI emplacement and are consistent with our estimates. Apparently, the fluorine- and boron-rich fluids circulated during and/or after the ignimbrite emplacement. Indeed, the xenoliths occur in the uppermost portion of the thick ignimbrite sequence and were not subjected to the density and size effects expected in pyroclastic flow currents. The secondary crystallization, as well as the contraction phenomena of some xenoliths described in the literature (Masi and Turi, 1972; Carati, 1987), was the consequence of metasomatic fluids acting on the carbonate xenoliths within the emplacing ignimbrite. This non-quantifiable phenomenon was likely the cause of the expected oxygen and carbon loss during the metasomatic process, as described in the literature (Bowman, 1998).

Based on the fluorophlogopite crystal chemistry and the isotope modelling, we suggest that hydrothermal fluids circulating in the pyroclastic flow were dominated by H_2O-rich fluids with only minor chlorine and fluorine. As the zeolite formation and the geochemistry of the micaceous xenoliths testify, these hot fluids were saline and likely provided F and B, as well as As and K, that were absent in both marbles and primary limestones (Table 4). Primary biotites of the CI have fluorine contents much lower (0.7 to 2.5 wt%, see the *Volcanological context* section above) than phlogopite of the Fiano xenoliths (up to 9.1 wt%; Table 3 and 6). Moreover, the glassy matrix was not able to trap fluorine, as their F contents overlap with those of the melt inclusions (0.26 to 0.89 wt%, see the *Volcanological context* section). Likewise, the CI rocks have B contents less than few tens of ppm (Tonarini *et al.*, 2004), not able to justify the up to ~ 9000 ppm measured in our xenoliths. Therefore, the enrichment in F and B, and possibly of other elements as As, with respect to both volcanic products and carbonate, may be related to their incompatible behaviour with respect to the magma and their partitioning into the gas phase of the eruption cloud.

The temperatures derived from isotope modelling agree with the stability condition of fluoborite and humite found in our xenoliths and strongly suggests that metasomatism of carbonates started contemporaneously with the circulation and release of fluids, with the zeolitization process starting afterwards.

Conclusions

Mineral chemistry, paragenesis and stable isotope geochemistry of xenoliths served as basis to investigate the physico-chemical conditions during the CI ignimbrite emplacement at the Fiano site (ca. 50 km far from the eruption source). The data of the present study, together with literature data, indicate infiltration of fluid enriched in F, B, Mg and As through dominantly water-rich fluids affecting the carbonate rocks starting from temperatures of ~ 300-450°C.

A suggestion for possible future investigations is modelling and quantitative evaluations of the environmental impact of hazardous elements. F, As and B have been immobilized by metamorphic reactions in the Fiano nodules. Further studies should quantify the possible local release and concentrations of F, As and B in soils, groundwater and atmosphere, with implications on the environmental impact of the eruption.

Acknowledgements

G. Balassone wishes to dedicate this work to the memory of Enrico Franco, inspiring Mineralogist and academic Teacher at the University of Naples (Italy). The accurate reviews of Ștefan Marincea and Gianluca Iezzi and the comments of Roger Mitchell and Pete Leverett greatly helped to improve the quality of the paper. Financial support to this research came from University of Naples 2014 fund granted to G.B. and from the COFIN MIUR

662 2010-2011 (2010EARRRZ_010) granted to University of Bari. Dr. R. de
663 Gennaro (DiSTAR, University of Naples) is thanked for help with SEM-
664 EDS analyses. V. Monetti and L.M. Francese (DiSTAR, University of
665 Naples) assisted with laboratory support. Prof. Stefano Poli and Andrea
666 Risplendente (University of Milan) are acknowledged for the facilities at the
667 Electron Microprobe Laboratory. Facilities at the Centro Interdipartimentale
668 Laboratorio di Ricerca per la Diagnostica dei Beni Culturali, University of
669 Bari, are also acknowledged.

670

671 **References**

672 Arienzo, I., Heumann, A., Wörner, G., Civetta, L. and Orsi, L. (2011)
673 Processes and timescales of magma evolution prior to the Campanian
674 Ignimbrite eruption (Campi Flegrei, Italy). *Earth and Planetary Science*
675 *Letters*, **306(3-4)**, 217-228.

676 Bachechi, F., Federico, M. and Fornaseri, M. (1966) La ludwigite e i
677 minerali che l'accompagnano nelle geodi delle "pozzolane nere" di
678 Corcolle (Tivoli, Colli Albani). *Periodico di Mineralogia*, **35**, 975-1022.

679 Balassone, G., Franco, E., Mattia, C.A., Petti, C. and Puliti, R. (2002) Re-
680 examination of fluosiderite, an unknown mineral from southern Italy:
681 equal to fluorine-rich chondrodite. *European Journal of Mineralogy*, **14**,
682 151-155.

683 Balassone, G., Scordari, F., Lacalamita, M., Schingaro, E., Mormone, A.,
684 Piochi, M., Petti, C. and Mondillo, N. (2013) Trioctahedral micas in
685 xenolithic ejecta from recent volcanism of the Somma-Vesuvius (Italy):
686 Crystal chemistry and genetic inferences. *Lithos*, **160-161**, 84-97.
687 Barberi, F. and Leoni, L. (1980) Metamorphic carbonate ejecta from
688 Vesuvius Plinian eruptions: Evidence of the occurrence of shallow
689 magma chambers. *Bullettin of Volcanology*, **43**, 107-120.
690 Betteridge, P.W., Carruthers, J.R., Cooper, R.I., Prout, K. and Watkin, D.J.
691 (2003) Crystals version 12: software for guided crystal structure analysis.
692 *Journal of Applied Crystallography*, **36**, 1487.
693 Bottinga, Y. (1968) Calculation of fractionation factors for carbon and
694 oxygen isotopic exchange in the system calcite-carbon dioxide-water.
695 *The Journal of Physical Chemistry*, **72**, 800-808.
696 Bowman, J.R. (1998) Stable-isotope systematics of skarns. Pp. 99-145 in:
697 *Mineralized intrusion-related skarn systems* (D.R. Lentz, editor). Short
698 Course Series, **26**. Mineralogical Association of Canada, Ottawa.
699 Brisi, C. and Eitel, W. (1957) Identity of nocerite and fluoborite. *American*
700 *Mineralogist*, **42 (3-4)**, 288-293.
701 Bruker (2007). SAINT, Bruker AXS Inc., Madison, Wisconsin, USA.
702 Bruker (2009). SADABS, Bruker AXS Inc., Madison, Wisconsin, USA.

Cámara, F. and Ottolini, L. (2000) New data on the crystal-chemistry of fluoborite by means of SREF, SIMS, and EMP analysis. *American Mineralogist*, **85**, 103-107.

Caponera, I., Fiori, S. and Pucci, R. (2003) Fluoborite, piombo nativo, richterite ed altri interessanti ritrovamenti nei Colli Albani. Il Cercapietre. *Notiziario del Gruppo Mineralogico Romano*, **1-2**, 3-13.

Cappelletti, P., Cerri, G., Colella, A., de' Gennaro, M., Langella, A., Perrotta, A. and Scarpati, C. (2003) Post-eruptive processes in the Campanian Ignimbrite. *Mineralogy and Petrology*, **79**, 79-97.

Carati, M. (1987) I minerali degli inclusi metamorfosati nel tufo grigio campano. *Notiziario del Gruppo Mineralogico Geologico Napoletano,* **18**, 6-13.

Cesare, B., Cruciani, G. and Russo, U. (2003) Hydrogen deficiency in Ti-rich biotite from anatectic metapelites (El Joyazo, SE Spain): Crystal-chemical aspects and implications for high-temperature petrogenesis. *American Mineralogist*, **88**, 583-595.

Civetta, L., Orsi, G., Pappalardo, L., Fisher, R.V., Heiken, G. and Ort, M. (1997) Geochemical zoning, mingling, eruptive dynamics and depositional processes – the Campanian Ignimbrite, Campi Flegrei caldera, Italy. *Journal of Volcanology and Geothermal Research,* **75**, 183-219.

724 Costa, A., Folch, A., Macedonio, G., Giaccio, B., Isaia, R. and Smith, V.C.
725 (2012) Quantifying volcanic ash dispersal and impact of the Campanian
726 Ignimbrite super-eruption. *Geophysical Research Letters*, **39(10)**, l-5.
727 de Gennaro, M., Calcaterra, D. and Langella, A. (2013) *Le pietre storiche*
728 *della Campania – dall'oblio alla riscoperta*. (Luciano, editor). Napoli,
729 Della Ventura, G., Parodi, G.C. and Maras, A. (1992) Potassium-fluor-
730 richterite, a new amphibole form San Vito, Monte Somma, Campania,
731 Italy. *Rendiconti dell'Accademia dei Lincei, Classe di Scienze Fisiche,*
732 *Maematiche e Naturali*, **9(3)**, 239-245.
733 Del Moro, A., Fulignati, P., Marianelli, P. and Sbrana, A. (2001) Magma
734 contamination by direct wall rock interaction, constraints from xenoliths
735 from the walls of a carbonate-hosted magma chamber (Vesuvius 1944
736 eruption). *Journal of Volcanology and Geothermal Research*, **112**, 15-24.
737 Droop G.T.R. (1987) A general equation for estimating Fe^{3+} concentrations
738 in ferromagnesian silicates and oxides from microprobe analysis, using
739 stoichiometric criteria. *Mineralogical Magazine*, **51**, 431-7.
740 Fedele, F.G., Giaccio, B., Isaia, R. and Orsi, G. (2002) Ecosystem impact of
741 the Campanian Ignimbrite eruption in Late Pleistocene Europe.
742 *Quaternary Research*, **57**, 420-424.
743 Fedele, L., Tarzia, M., Belkin, H.E., De Vivo, B., Lima, A. and Lowenstern,
744 J.B. (2006) Magmatic-hydrothermal fluid interaction and mineralization
745 in alkali-syenite nodules from the Breccia Museo pyroclastic deposit,

746 Naples, Italy. Pp. 125-161 in: *Volcanism in Campania Plain: Vesuvius,*
747 *Campi Flegrei and Ignimbrites* (B. De Vivo, editor). Developments in
748 Volcanology, **9**. Elsevier.
749 Fedele, L., Scarpati, C., Marvin, L., Melluso, L., Morra, V. Perrotta, A. and
750 Ricci, G. (2008) The Breccia Museo formation, Campi Flegrei, southern
751 Italy: geochronology, chemostratigraphy and relationship with the
752 Campanian Ignimbrite eruption. *Bulletin of Volcanology*, **10**, 1189-1219.
753 Fisher, R. V., Orsi, G., Ort, M. and Heiken, G. (1993) Mobility of a large-
754 volume pyroclastic flow-emplacement of the Campanian ignimbrite, Italy.
755 *Journal of Volcanology and Geothermal Research*, **56(3)**, 205-220.
756 Flamini, A., Graziani, G. and Pagliuca, G. (1979) Synthesis of the fluorine
757 end member of the fluoborite series. *American Mineralogist*, **64**, 229-231.
758 Fulignati, P., Panichi, C., Sbrana, A., Caliro, S., Gioncada, A. and Del Moro,
759 A. (2005) Skarn formation at the walls of the 79AD magma chamber of
760 Vesuvius (Italy): Mineralogical and isotopic constraints. *Neues Jahrbuch*
761 *für Mineralogie Abhandlungen*, **181(1)**, 53-66.
762 Giaccio, B., Isaia, R., Fedele, F.G., Di Canzio, E., Hoffecker, J., Ronchitelli,
763 A., Sinitsyn, A.A., Anikovich, M,, Lisitsyn, S.N. and Popov, V.V. (2008)
764 The Campanian Ignimbrite and Codola tephra layers: Two
765 temporal/stratigraphic markers for the Early Upper Palaeolithic in
766 southern Italy and eastern Europe. *Journal of Volcanology and*
767 *Geothermal Research*, **177**, 208-226.

768 Gianfagna, A., Scordari, F., Mazziotti-Tagliani, S., Ventruti, G. and Ottolini,
769 L. (2007) Fluorophlogopite from Biancavilla (Mt. Etna, Sicily, Italy):
770 Crystal structure and crystal chemistry of a new F-dominant analog of
771 phlogopite. *American Mineralogist*, **92**, 1601-1609.
772 Gilg, H.A., Lima, A., Somma, R., Belkin, H.E., De Vivo, B. and Ayuso,
773 R.A. (2001) Isotope geochemistry and fluid inclusion study of skarns
774 from Vesuvius. *Mineralogy and Petrology*, **73**, 145-176.
775 Hawthorne F.C., Oberti R., Harlow G.E., Maresch W.V., Martin R.F.,
776 Schumacer J.C., Welch M.D. (2012) Nomenclature of the amphibole
777 supergroup. *American Mineralogist*, **97**, 2031–2048.
778 Hazen, R.M. and Burnham, C.W. (1973) The crystal structures of one-layer
779 phlogopite and annite. *American Mineralogist*, **58**, 889-900.
780 Hazen, R.M., Finger, L.W. and Velde, D. (1981) Crystal structure of a
781 silica- and alkali-rich trioctahedral mica. *American Mineralogist*, **66**,
782 586-591.
783 Heinrich, W. (1994) Potassium-fluor-richterite in metacherts from the Bufa
784 del Diente contact-metamorphic aureole, NE-Mexico. *Mineralogy and*
785 *Petrology*, **50**, 259-270.
786 Iannace, A. (1991) Ambienti deposizionali e processi diagenetici in
787 successioni di piattaforma carbonatica del Trias Superiore nei Monti
788 Lattari e Picentini (Salerno). *PhD Thesis, Università di Napoli "Federico*
789 *II", Naples, Italy.*

790 Joswig, V.W. (1972) Neutronenbeugungsmessungen an einem 1*M*-
791 Phlogopit. *Neues Jahrbuch für Mineralogie,Monatshefte*, 1-11.
792 Lacalamita, M., Schingaro, E., Scordari, F., Ventruti, G., Fabbrizio, A. and
793 Pedrazzi, G. (2011) Substitution mechanisms and implications for the
794 estimate of water fugacity for Ti-rich phlogopite from Mt. Vulture
795 (Potenza, Italy). *American Mineralogist*, **96**, 1381-1391.
796 Langella, A., Bish, D.L., Cappelletti, P., Cerri, G., Colella, A., de Gennaro,
797 R., Graziano, S.F., Perrotta, A., Scarpati, C. and de Gennaro, M. (2013)
798 New insights into the mineralogical facies distribution of Campanian
799 Ignimbrite, a relevant Italian industrial material. *Applied Clay Science*,
800 **72**, 55-73.
801 Leeman, W.P., Sisson, V.B. and Reid, M.R. (1992) Boron geochemistry of
802 the lower crust: evidence from granulite terranes and deep crustal
803 xenoliths. *Geochimica et Cosmochimica Acta*, **56**, 775-788.
804 Marianelli, P., Sbrana, A. and Proto, M. (2006) Magma chamber of the
805 Campi Flegrei supervolcano at the time of eruption of the Campanian
806 Ignimbrite. *Geology*, **34(11)**, 937-940.
807 Marincea, Ş. (2000) Fluoborite in magnesian skarns from Baita Bihor
808 (Bihor Massif, Apuseni Mountains, Romania). *Neues Jahrbuch für*
809 *Mineralogie, Monatshefte*, **8**, 357-371.
810 Masi, U. and Turi, B. (1972) Frazionamento isotopico del carbonio e
811 dell'ossigeno negli inclusi calcarei metamorfosati del "Tufo grigio

campano" Auct. di Fiano (Salerno). *Periodico di Mineralogia*, **41**, 291-310.

McCauley, J.W., Newnham, R.E. and Gibbs, G.V. (1973) Crystal structure analysis of synthetic fluorophlogopite. *American Mineralogist*, **58**, 249-254.

McDonough, W.F. and Sun, S.S. (1995) The Composition of the Earth. *Chemical Geology*, **120**, 223-253.

Ort, M.H, Rosi, M. and Anderson, C.D. (1999) Correlation of deposits and vent locations of the proximal Campanian Ignimbrite deposits, Campi Flegrei, Italy, based on natural remanent magnetization and anisotropy of magnetic susceptibility characteristics. *Journal of Volcanology and Geothermal Research*, **91**, 167-178.

Ottolini, L., Schingaro, E. and Scordari, F. (2012) Ceramics: Contribution of Secondary Ion Mass Spectrometry (SIMS) to the Study of Crystal Chemistry of Mica Minerals. Pp. 1017-1060 in: *Mass Spectrometry Handbook*. Wiley Series on Pharmaceutical Science and Bioteechnology: Practices, Applications, and Methods, **43**. J. Wiley & Sons, Hoboken, NJ, USA.

Pappalardo, L., Ottolini, L. and Mastrolorenzo, G. (2008) The Campanian Ignimbrite (southern Italy) geochemical zoning: insight on the generation of a super-eruption from catastrophic differentiation and fast withdrawal. *Contribution to Mineralogy and Petrology*, **156(1)**, 1-26.

834 Piochi, M., Bruno, P.P. and De Astis, G. (2005) Relative roles of rifting
835 tectonics and magma ascent processes: inferences from geophysical,
836 structural, volcanological, and geochemical data of the Neapolitan
837 volcanic region (southern Italy). *Geochemistry, Geophysics, Geosystems*,
838 **6(7)**, 1-25.
839 Piochi, M., Polacci, M., De Astis, G., Zanetti, A., Mangiacapra, A.,
840 Vannucci, R. and Giordano, D. (2008) Texture and composition of
841 pumices and scoriae from the Campi Flegrei caldera (Italy): Implications
842 on the dynamics of explosive eruptions. *Geochemistry Geophysics*
843 *Geosystems*, **9(3)**, 1-25.
844 Piochi, M., Mormone, A., Balassone, G., Strauss, H., Troise, C. and De
845 Natale, G. (2015) Native sulfur, sulfates and sulfides from the active
846 Campi Flegrei volcano (southern Italy): Genetic environments and
847 degassing dynamics revealed by mineralogy and isotope geochemistry.
848 *Journal of Volcanology and Geothermal Research*, **304**, 180-193.
849 Polacci, M., Pioli, L. and Rosi, M. (2003) The Plinian phase of the
850 Campanian Ignimbrite eruption (Phlegrean Fields, Italy): evidence from
851 density measurements and textural characterization of pumice. *Bulletin of*
852 *Volcanology*, **65**, 418-432.
853 Redhammer, G.J. and Roth, G. (2002) Single-crystal structure refinements
854 and crystal chemistry of synthetic trioctahedral micas $KM_3(Al^{3+}$,

$Si^{4+})_4O_{10}(OH)_2$, where M = Ni^{2+}, Mg^{2+}, Co^{2+}, Fe^{2+}, or Al^{3+}. *American Mineralogist*, **87**, 1464-1476.

Rosen, O., Desmons, J. and Fettes, D. (2007) A systematic nomenclature for metamorphic rocks. 7. Metacarbonates and related rocks. Recommendations by the IUGS Subcommission on the systematics of metamorphic rocks. SCMR website (www.bgs.ac.uk/SCMR).

Russell, R.L. and Guggenheim, S. (1999) Crystal structures of near-end-member phlogopite at high temperatures and heat-treated Fe-rich phlogopite; the influence of the O, OH, F site. *Canadian Mineralogist*, **37(3)**, 711-720.

Scacchi, A. (1888) La regione vulcanica fluorifera della Campania. *Atti della Reale Accademia delle Scienze Fisiche e Matematiche di Napoli*, **2(2)**, 1-108.

Scacchi, A. (1890) La regione vulcanica fluorifera della Campania. *Memorie Regio Comitato Geologico Italiano, Estratti*, **IV(I)**, 1-48.

Schingaro, E., Lacalamita, M., Scordari, F., Brigatti, M.F. and Pedrazzi, G., (2011) Crystal chemistry of Ti-rich fluorophlogopite from Presidente Olegario, Alto Paranaíba igneous province, Brazil. *American Mineralogist*, **96**, 732-743.

Schingaro, E., Lacalamita, M., Scordari, F. and Mesto, E. (2013) 3*T*-phlogopite from Kasenyi kamafugite (SW Uganda): EPMA, XPS, FTIR, and SCXRD study. *American Mineralogist*, **98**, 709-717.

877 Schingaro, E., Kullerud, K., Lacalamita, M., Mesto, E., Scordari, F.,
878 Zozulya, D., Erambert, M. and Ravna, E.J.K. (2014) Yangzhumingite
879 and phlogopite from the Kvaløya lamproite (North Norway): Structure,
880 composition and origin. *Lithos*, **210-211**, 1-13.
881 Scordari, F., Schingaro, E., Ventruti, G., Nicotra, E., Viccaro, M. and
882 Mazziotti Tagliani, S. (2013) Fluorophlogopite from Piano delle
883 Concazze (Mt. Etna, Italy): crystal chemistry and implications for the
884 crystallization conditions. *American Mineralogist*, **98**, 1017-1025.
885 Shannon, R.D. (1976) Revised effective ionic radii and systematic studies of
886 interatomic distances in halides and chalcogenides. *Acta*
887 *Crystallogaphica*, **A32**, 751-767.
888 Signorelli, S., Vaggelli, G., Romano, C. and Carroll, M.R. (2001) Volatile
889 element zonation in Campanian Ignimbrite magmas (Phlegrean Fields,
890 Italy): evidence from the study of glass inclusions and matrix glasses.
891 *Contribution to Mineralogy and Petrology*, **140(5)**, 543-553.
892 Takeda, H. and Donnay, J.D.H. (1966) Trioctahedral One-Layer Micas. III.
893 Crystal Structure of a Synthetic Lithium Fluormica. *Acta*
894 *Crystallographica*, **A20**, 638-646.
895 Takeda, H. and Morosin, B. (1975) Comparison of observed and predicted
896 structural parameters of mica at high temperature. *Acta*
897 *Crystallographica*, **B31**, 2444-2452.

898 Taylor, H.P., Giannetti B, Turi B (1979) Oxygen isotope geochemistry of
899 the potassic igneous rocks from the Roccamonfina volcano, Roman
900 comagmatic region, Italy. Earth and Planetary Science Letters 46: 81-
901 106.
902 Tell, I. (1974) Hydrothermal Studies on Fluorine Metamorphic Reactions in
903 Siliceous Dolomite. *Contribution to Mineralogy and Petrology*, **43**, 99-
904 110.
905 Tomlinson, E.L., Arienzo, I., Civetta, L., Wulf, S., Smith, V.C., Hardiman,
906 M., Lane, C.S., Carandente, A., Orsi, G., Rosi, M., Müller, W. and
907 Menzies, M.A. (2012) Geochemistry of the Phlegraean Fields (Italy)
908 proximal sources for major Mediterranean tephras: Implications for the
909 dispersal of Plinian and co-ignimbritic components of explosive
910 eruptions. *Geochimica et Cosmochimica Acta*, **93**, 102-128.
911 Tonarini, S., Leeman, W.P., Civetta, L., D'Antonio, M., Ferrara, G. and
912 Necco, A. (2004) B/Nb and $\delta^{11}B$ systematics in the Phlegrean Volcanic
913 District, Italy. *Journal of Volcanology and Geothermal Research*, **133**,
914 123-139.
915 Turi, B. (1969) Carbon and oxygen isotopic composition of carbonates in
916 limestones blocks and related geodes from the "Black Pozzolans"
917 formation of the Alban Hills. *Chemical Geology*, **5**, 195-205.

Vitale, S. and Isaia, R. (2014) Fractures and faults in volcanic rocks (Campi Flegrei, southern Italy): insight into volcano-tectonic processes. *International Journal of Earth Sciences*, **103**, 801-819.

Weiss, Z., Rieder, M. and Chmielová, M. (1992) Deformation of coordination polyhedra and their sheets in phyllosilicates. *European Journal of Mineralogy*, **4**, 665-682.

White, J.S. (1981) Grothine discredited, equals norbergite. *The Mineralogical Record*, **12(6)**, 377-378.

Whitney D.L. and Evans B.W. (2010) Abbreviations for names of rock-forming minerals. *American Mineralogist*, **95**, 185-187.

Zambonini, F. (1919) Il tufo pipernoide della Campania e i suoi minerali. *Memorie per servire alla Descrizione della Carta Geologica d'Italia*, **7**, pp. 130.

Zheng, Y.F. (1990) Carbon-oxygen isotopic covariation in hydrothermal calcite during degassing of CO_2. A quantitative evaluation and application to the Kushikino gold mining area in Japan. *Mineralium Deposita*, **25(4)**, 246-250.

Zheng, Y.F. and Hoefs, J. (1993) Carbon and oxygen isotope covariations in hydrothermal calcites. *Mineralium Deposita*, **28**, 79-89.

Figure captions

939 **FIG. 1.** Map of the Campania region, showing the extent of the Campanian
940 Ignimbrite outcrops (modified after Arienzo *et al.*, 2011), as well as the
941 Phlegraean and Somma-Vesuvius volcanic areas; the sampling location at
942 Fiano is indicated by a yellow star. The top right inset illustrates the extent
943 of the Campanian Ignimbrite tephra in south-eastern Europe within its limits
944 of preservation (Fedele *et al.*, 2008).
945
946 **FIG. 2.** (*a*) The Fiano quarries (the so called "*Tufare*") for extraction of the
947 Campanian Ignimbrite (CI), as appeared at the beginning of the 20th century
948 (after Zambonini, 1919). Grey tuff is at the base, overlaid by alternating
949 layers of grey and yellow tuffs, with big limestone blocks. (*b*) CI outcrops
950 nowadays, with the grey tuff showing the remains of the old mining activity
951 (courtesy of P. Kastenmeier).
952
953 **FIG. 3.** (*a*) A typical fluorophlogopite-bearing sample from Fiano. (*b*) SEM
954 image of an aggregate of fluoborite (Flb), fluorophlogopite (Phl) and
955 fluorite (Fl).
956
957 **FIG. 4.** SEM-BSE micrographs of the mineral assemblage of the Fiano
958 xenoliths. (*a*) fluorophlogopite (Phl) and fluorite (Fl) (sample TF2); (*b*)
959 fluorophlogopite with interstitial fluorite and magnetite (Mag) (sample
960 TF2); (*c*) K-bearing fluoro-richterite (Rct) and fluorite (sample TF2); (*d*)

fluorophlogopite, fluorite and magnesioferrite (Mfr) (sample TF4); (*e*) fluoborite (Flb) in needle-like crystals and fluorite (sample TF6); (*f*) enlargement of the previous micrograph; (*g*) chondrodite (Chn) and fluorite, with tiny magnetite crystals (sample TF12); (*h*) diopside (Di), fluorophlogopite and fluorite, with magnetite in both euhedral and tiny anhedral individuals (sample TF12).

FIG. 5. REE pattern distributions for the studied xenoliths (red and yellow diamonds for the micaceous and carbonate xenoliths, respectively) in the field of Somma-Vesuvius marble and unmetamorphosed limestone (Del Moro *et al.,* 2001) compared with data from whole-rocks (unfilled circle: data from Civetta *et al.,* 1997), melt inclusions (filled circles: data from Marianelli *et al.,* 2006) and glassy matrix (filled squares: data from Civetta *et al.,* 1997) of the CI. Values normalized on the basis of McDonough and Sun (1995).

FIG. 6. Plot of carbon versus oxygen isotope values of the Fiano xenoliths and comparison with literature data. The "thermal metamorphism" field depicts the range of isotopic compositions of calcites from metalimestones, metadolostones and skarns of Somma-Vesuvius after Gilg *et al.* (2001), and some of the metamophosed Fiano xenoliths after Masi and Turi (1972); the "weathering" field represents the isotopic composition of outer shells of the

983 Fiano xenoliths affected by exchange process with meteoric water (Masi
984 and Turi, 1972). The range of $\delta^{18}O$ for CI whole rocks and feldspar from
985 Taylor et al. (1979) is also reported. See text for further discussion.
986
987 **FIG. 7.** Plot of ditrigonalization parameter (α) *vs.* F content for micas
988 affected by variable extent of $OH^- \rightarrow F^-$ substitution. Symbols: Solid
989 diamonds indicate the phlogopites in this study: red for the TF2; green for
990 the TF7; blue for the TF10 crystals. Open symbols for literature
991 fluorophlogopites (square: Takeda and Donnay, 1966; circle: Joswig, 1972;
992 triangle pointing upward: Hazen and Burnham, 1973; triangle pointing
993 downward: McCauley *et al.,* 1973; diamond: Takeda and Morosin, 1975;
994 square with plus inside: Hazen *et al.,* 1981; circle with plus inside: Russell
995 and Guggenheim, 1999; triangle pointing upward with plus inside:
996 Gianfagna *et al.,* 2007; triangle pointing downward with plus inside:
997 Schingaro *et al.,* 2011; diamond with plus inside: Scordari *et al.,* 2013; star:
998 Schingaro *et al.,* 2014; square, circle, triangle pointing upward and triangle
999 pointing downward with horizontal line: Balassone *et al.,* 2013). Open
1000 symbols with vertical bar inside for literature de-hydrogenated phlogopites
1001 and end member phlogopite (square: Redhammer and Roth, 2002; circle:
1002 Cesare *et al.,* 2003). Open symbols with cross inside are phlogopites from
1003 Balassone *et al.* (2013).
1004

FIG. 8. Covariation of C and O isotope composition as from modelling of interaction between an initial sedimentary carbonate (limestone with $\delta^{13}C$ = 0.79‰ VPDB and $\delta^{18}O$ = 30‰ VSMOW, average from Iannace, 1991) and a hydrothermal fluid with $\delta^{13}C$ = -13‰ VPDB and $\delta^{18}O$ = 8‰ VSMOW in the temperature range 100-350°C (as derived by mineralogical data), or a magmatic fluid with $\delta^{13}C$ = 0‰ VPDB and $\delta^{18}O$ = 10‰ VSMOW at 750°C (following Fulignati *et al.*, 2005). Modelling made following Zheng and Hoefs (1993). Points along the lines are the fluid/rock ratio from 0 at the not modified limestone value to 1 at the opposite side as maximum exchange. The plot also shows the decarbonation modelling through Rayleigh processes (Bowman, 1998). In such a case, points along the lines indicate element (O, C) fractionation from any, e.g. 0.01, to maximum possible, e.g. 1, isotope fractionation. For calculation we used equilibrium isotopic fractioning values α =$(1000+\delta^{13}C)$calcite/$(1000+\delta^{13}C)$fluid and $1000+\delta^{18}O)$calcite/$(1000+\delta^{18}O)$fluid fluid properly recalculated as a function of temperature after Bottinga (1968), in the various systems: $CaCO_3$-H_2O and $CaCO_3$-HCO_3 for the exchanges at 100° and 350°C, $CaCO_3$-H_2O and $CaCO_3$-CO_2, for the exchanges at 750°C, and $CaCO_3$-CO_2 for decarbonation.

FIG. 9. Calculated $10^3 \ln \alpha$ versus oxygen (*a*) and carbon (*b*) fractionation recalculated considering decarbonation of the initial carbonate (average

1027 from Iannace, 1991) and determined values of $\delta^{18}O$ and $\delta^{13}C$. Modelling is
1028 carried out using the formula of Zheng and Hoefs (1993) and Bowman
1029 (1998), whereas the temperatures on the right side of the diagrams are
1030 derived from Bottinga (1968) based on equilibrium isotopic fractioning
1031 values α as in Fig. 8.

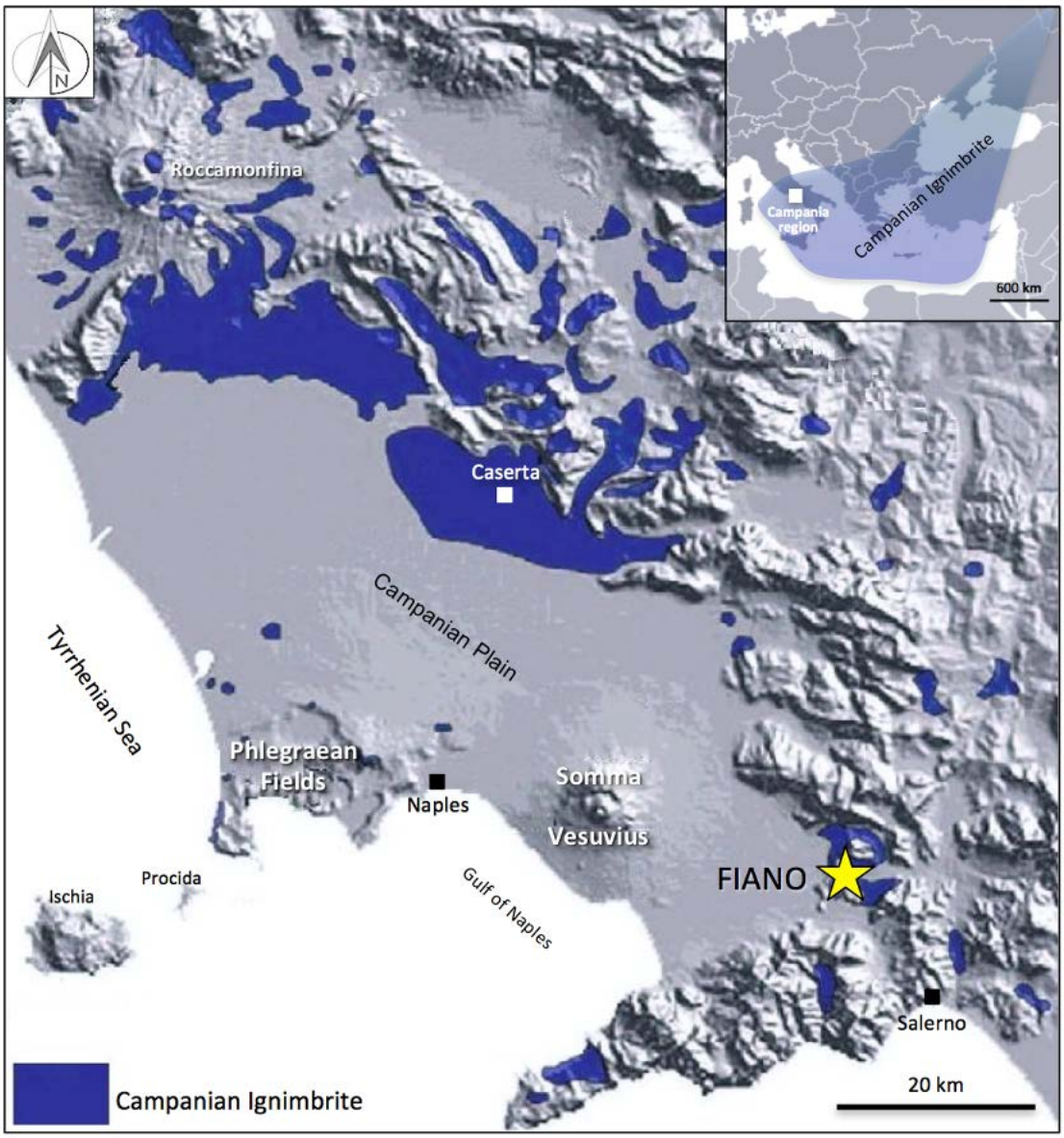

This is a 'preproof' accepted article for Mineralogical Magazine.
This version may be subject to change during the production process.
10.1180/minmag.2016.080.155

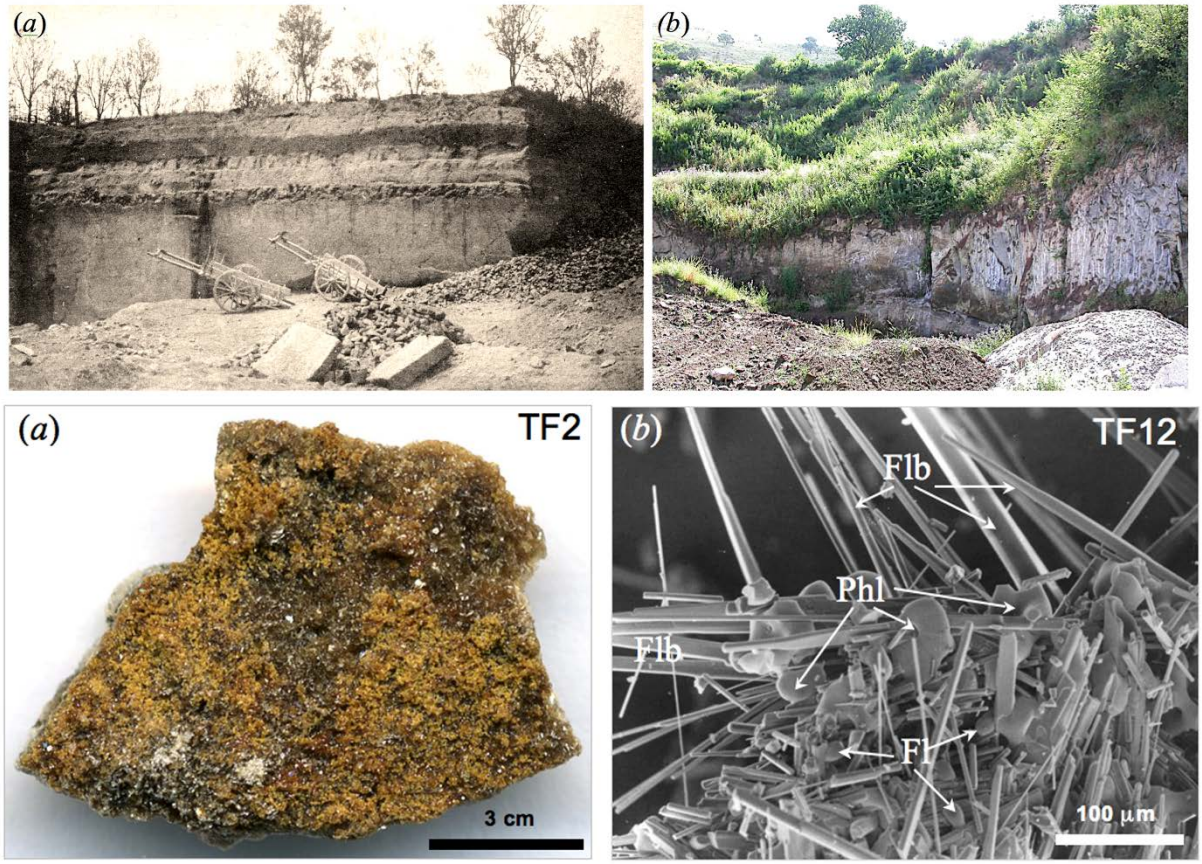

Fig. 3

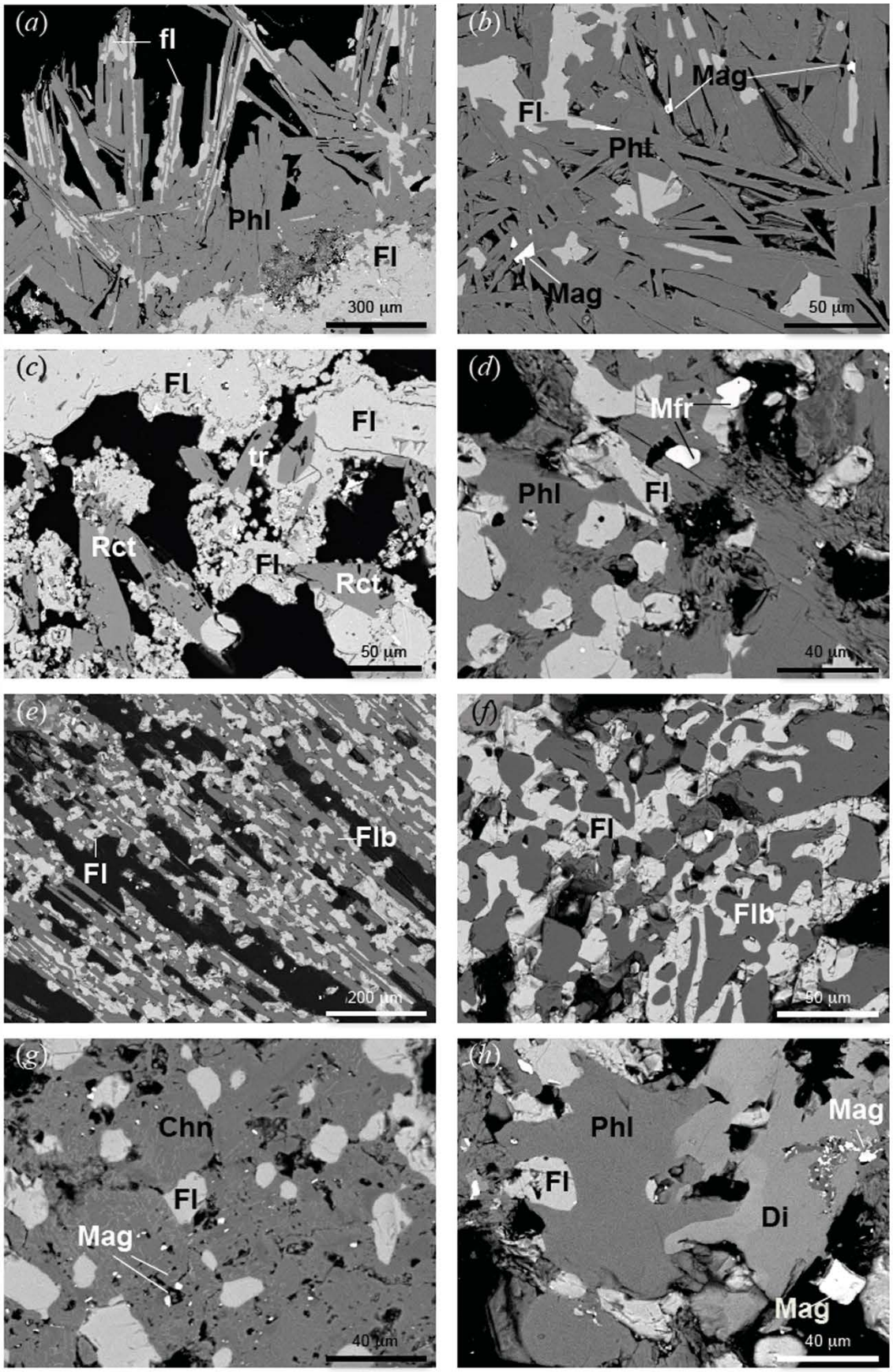

Fig. 4

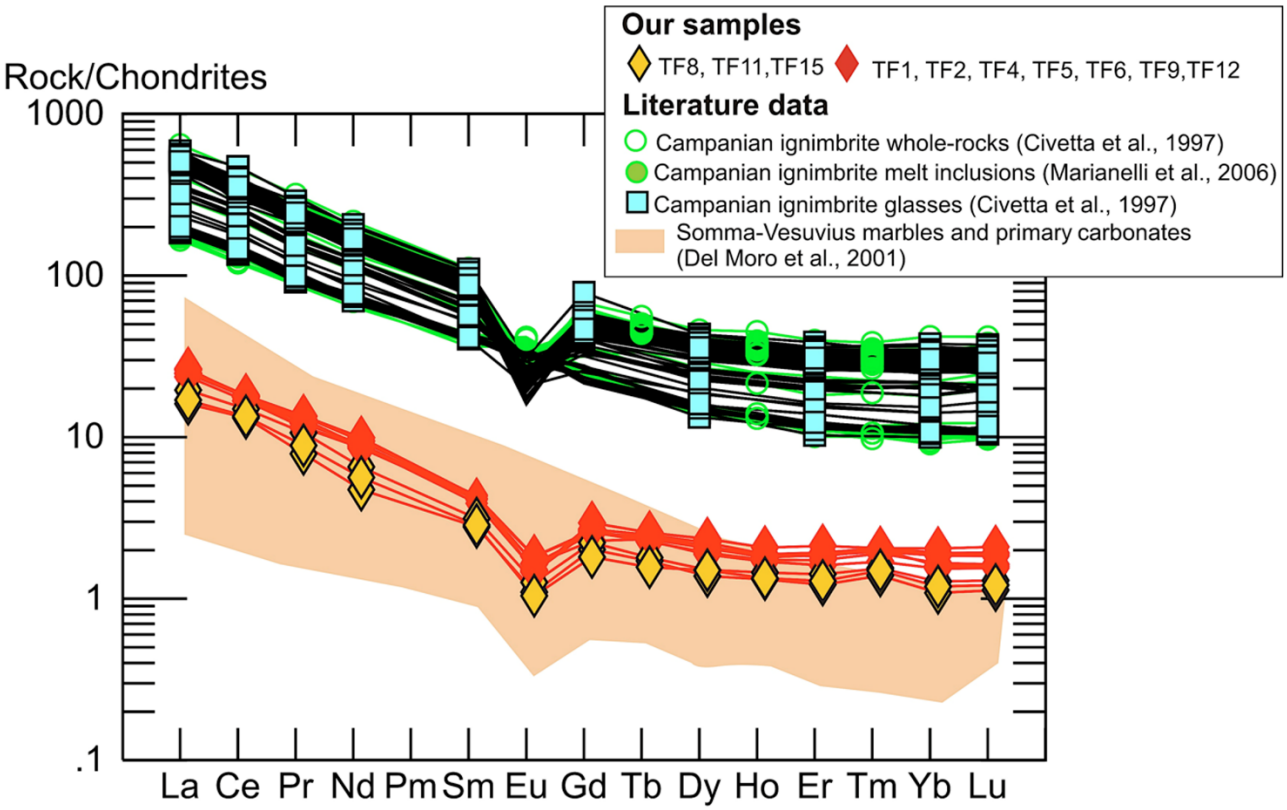

Fig. 5

This is a 'preproof' accepted article for Mineralogical Magazine.
This version may be subject to change during the production process.
10.1180/minmag.2016.080.155

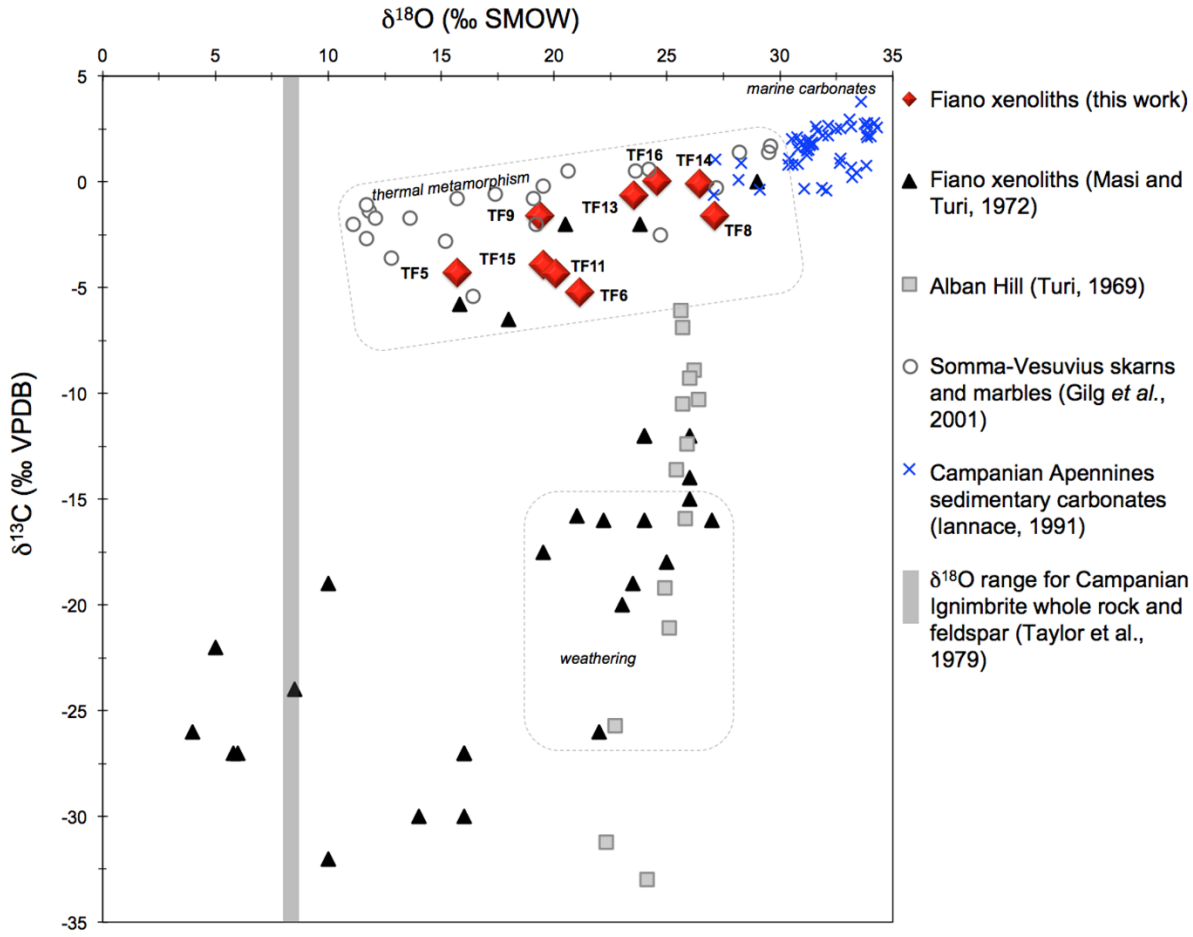

Fig. 6

This is a 'preproof' accepted article for Mineralogical Magazine.
This version may be subject to change during the production process.
10.1180/minmag.2016.080.155

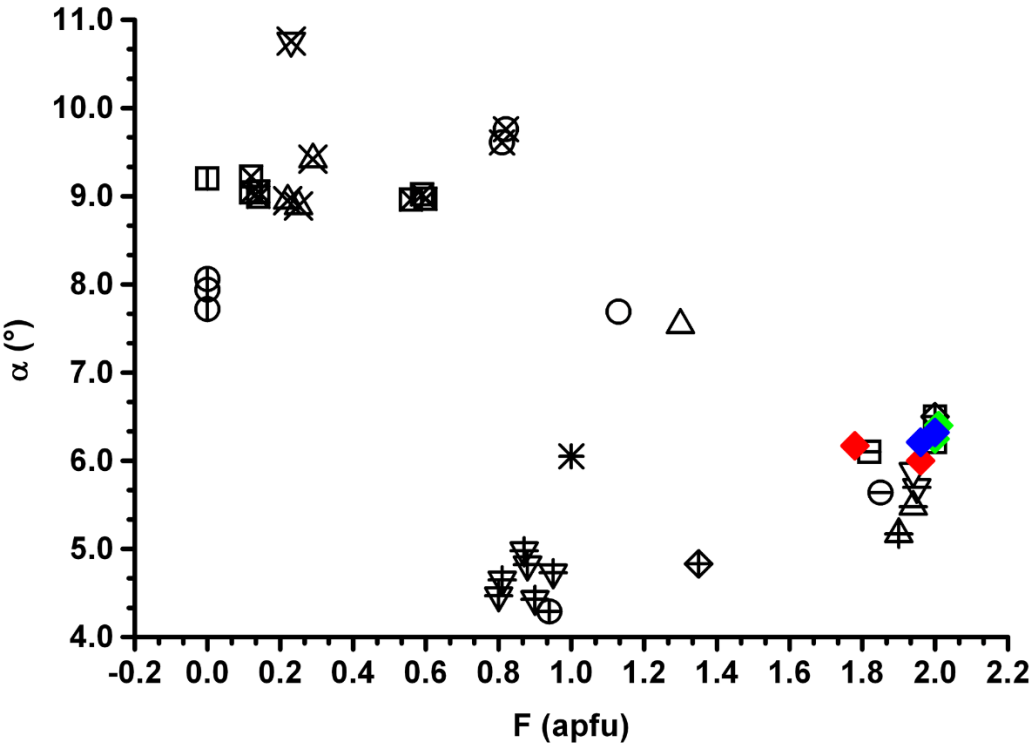

This is a 'preproof' accepted article for Mineralogical Magazine.
This version may be subject to change during the production process.
10.1180/minmag.2016.080.155

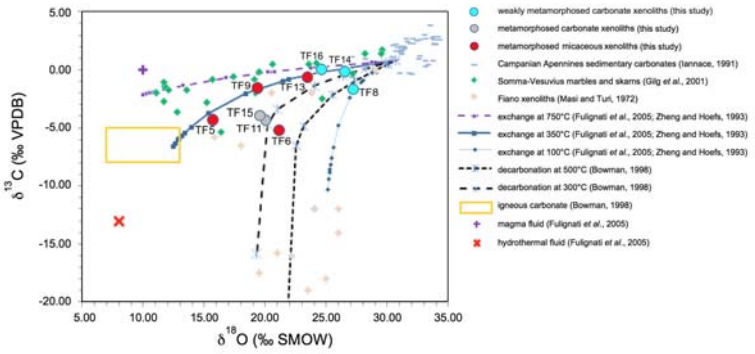

This is a 'preproof' accepted article for Mineralogical Magazine.
This version may be subject to change during the production process.
10.1180/minmag.2016.080.155

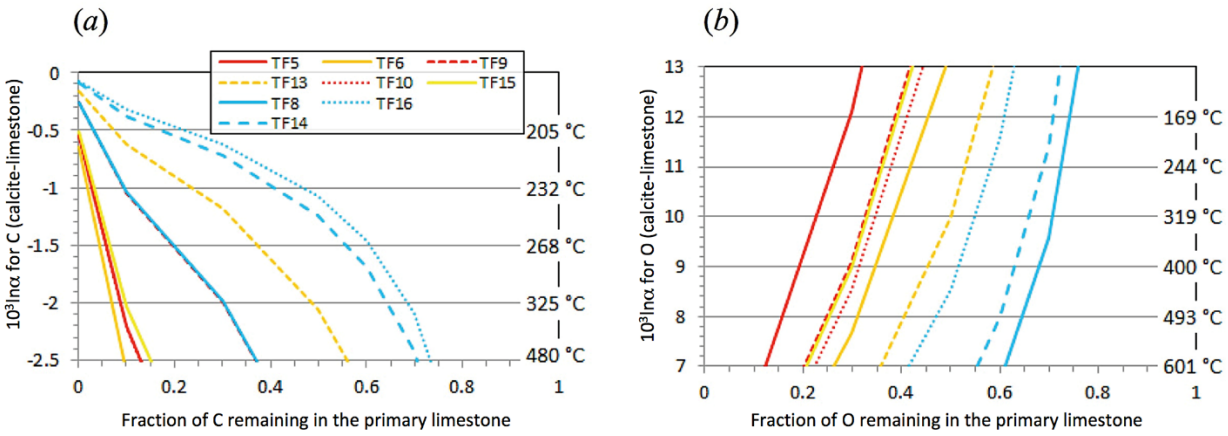

This is a 'preproof' accepted article for Mineralogical Magazine.
This version may be subject to change during the production process.
10.1180/minmag.2016.080.155

TABLE 1. An overall list of ideal crystal-chemical formulas of minerals found in the Fiano xenoliths, deriving from both this study and literature (Masi and Turi, 1972; Carati, 1987, and reference therein). Phases in italics are found in the investigated samples.

Minerals	Ideal formulas*
aragonite, *calcite*	$CaCO_3$
augite	$(Ca,Na)(Mg,Fe,Al,Ti)(Si,Al)_2O_6$
biotite	$K(Mg,Fe^{2+})_3AlSi_3O_{10}(OH,F)_2$
chondrodite	$(Mg,Fe^{2+})_5(SiO_4)_2(F,OH)_2$
diopside	$CaMgSi_2O_6$
fluoborite	$Mg_3(BO_3)(F,OH)_3$
fluorite	CaF_2
fluorophlogopite	$KMg_3(AlSi_3)O_{10}F_2$
*fluoro-richterite***	$Na(NaCa)Mg_5[Si_8O_{22}]F_2$
grossular	$Ca_3Al_2(SiO_4)_3$
hematite	Fe_2O_3
hornblende	$Ca_2(Mg,Fe^{2+})_4(Al,Fe^{3+})Si_7AlO_{22}(OH)_2$
hörnesite	$Mg_3(AsO_4)_2{\cdot}8(H_2O)$
humite	$Mg_7(SiO_4)_3(F,OH)_2$
hydromagnesite	$Mg_5(CO_3)_4(OH)_2{\cdot}4(H_2O)$
*magnesioferrite***	$MgFe_2O_4$
magnetite	$Fe^{2+}Fe^{3+}{}_2O_4$
marialite	$Na_4Al_3Si_9O_{24}Cl$
microsommite	$(Na,Ca,K)_{7\text{-}8}(Si,Al)_{12}O_{24}(Cl,SO_4)_{2\text{-}3}$
norbergite	$Mg_3SiO_4F_2$
periclase	MgO
sanidine	$KAlSi_3O_8$
sellaite	MgF_2
spinel	$MgAl_2O_4$
vanadinite	$Pb_5(VO_4)_3Cl$
vonsenite	$Fe^{2+}{}_2Fe^{3+}O_2(BO_3)$

*From http://rruff.info/ima/#. **Detected for the first time in the samples from this study.

TABLE 2. Sample label, rock description and associations of the Fiano samples, with minerals listed in order of decreasing abundance.

Sample ID	Rock sample description	Mineral assemblage*
Micaceous xenoliths		
TF1	micaceous xenolith, with red crust	Chn, Phl, Mag, Hem, Grs
TF2	honey-brown micaceous xenolith, with small red crusts	Phl, Fl, Chn, Di, Mag, Rct
TF4	honey-brown micaceous xenolith, with small red crusts	Fl, Phl, Chn, Flb, Di, Mag, Mfr
TF5	micaceous xenolith, with brown and red crusts on a small whitish nucleus	Phl, Fl, Chn, Flb, Di, Cal, Hu, Mag
TF6	micaceous xenolith, with brown and red crusts on a whitish nucleus	Fl, Phl, Flb, Chn, Di, Mag, Cal
TF7	honey-brown micaceous xenolith	Phl, Fl, Mag, Hem, Rct
TF9	micaceous xenolith, with a small white crust	Fl, Phl, Flb, Mag, Hem, Cal
TF10	micaceous xenolith, with red crust	Phl, Fl, Chn, Rct, Hem
TF12	micaceous xenolith, with red crust	Fl, Phl, Chn, Flb, Di, Mag, Mfr
TF13	micaceous xenolith, with red and white crust	Fl, Phl, Chn, Cal, Mag
Carbonate xenoliths		
TF8	poorly metamorphosed carbonate xenolith	Cal
TF11	metamorphosed carbonate xenolith	Cal, Fl, Hem
TF14	poorly metamorphosed carbonate xenolith	Cal
TF15	metamorphosed carbonate xenolith	Cal, Fl, Hem
TF16	poorly metamorphosed carbonate xenolith	Cal

*Cal, calcite; Chn, chondrodite; Di, diopside; Flb, fluoborite; Fl, fluorite; Rct, K-bearing fluoro-richterite; Grs, grossular; Phl, phlogopite; Hem, hematite; Hu, humite; Mag, magnetite; Mfr, magnesioferrite (symbols mainly after Whitney and Evans, 2010).

TABLE 3. Chemical composition (average EDS analyses on six to ten point-analysis, wt. %) and related structural formulae (atoms per formula units) of silicates (a) and non silicates (b) found in the Fiano xenoliths.

(a)

chondrodite		diopside		K-bearing fluoro-richterite		grossular		humite	
SiO_2	33.08	SiO_2	52.85	SiO_2	55.73	SiO_2	39.22	SiO_2	33.04
FeO_t	5.62	FeO_t	6.84	Al_2O_3	0.35	Al_2O_3	22.53	TiO_2	0.29
MgO	54.04	MgO	14.09	FeO_t	1.04	FeO_t	0.45	FeO_t	19.34
MnO	1.05	MnO	0.81	MgO	22.9	MgO	0.13	MgO	41.98
F	10.86	CaO	25.27	MnO	0.26	MnO	0.11	MnO	0.33
Total	104.65	Total	99.86	CaO	10.87	CaO	36.92	CaO	0.09
O=F				K_2O	1.42	Total	99.36	F	5.81
				Na_2O	4.13			Total	100.88
				F	4.57			O=F	-2.44
				Total	101.27			Total	98.44
				O=F	-1.92				
				Total	99.35				
10 (O, OH, F)		6 O		24 (O, OH, F)		24 O		14 (O, OH, F)	
Si	1.95	Si	1.79	Si	7.82	Si	5.94	Si	2.99
Fe	0.28	Fe	0.19	Al^{IV}	0.06	Al^{IV}	0.06	Ti	0.02
Mg	4.75	Mg	0.71	Fe	0.12	A^{IVI}	3.96	Fe	1.46
Mn	0.05	Mn	0.02	Mg	4.79	Fe	0.06	Mg	5.66
F	2.03	Ca	0.92	Mn	0.03	Mg	0.03	Mn	0.03
				Ca	1.63	Mn	0.01	Ca	0.01
				K	0.25	Ca	5.99	F	1.66
				Na	1.12				
				F	2.03				

(b)

calcite		fluoborite		fluorite		hematite		magnesioferrite[§]		magnetite[§]	
CaO	54.67	MgO	64.03	Ca	51.00	Fe_2O_3	95.68	Fe_2O_3	74.3	Fe_2O_3	67.57
MgO	0.66	CaO	0.03	Mg	0.12	Al_2O_3	2.91	FeO	0.2	FeO	29.14
MnO	0.14	$B_2O_3^*$	17.30	F	48.00	TiO_2	0.57	Al_2O_3	4.34	Al_2O_3	0.99
FeO	0.49	F	24.33	Total	99.12	Total	99.16	MgO	18.05	MgO	0.73
CO_2^*	43.71	H_2O^{**}	2.40					MnO	4.08	MnO	0.45
Total	99.18	Total	108.09					Total	100.97	CaO	0.21
		O=F	-10.24							Total	99.09
		Total	97.85								
2 O		1 B and 3 O				3 O		3 cations		3 cations	
Ca	1.95	Mg	3.07	Ca	1.00	Fe	1.90	Fe^{3+}	1.83	Fe^{3+}	1.96
Mg	0.03	Ca	0.001	Mg	0.004	Al	0.09	Fe^{2+}	0.005	Fe^{2+}	0.94
Mn	0.004	B	1.00	F	1.99	Ti	0.10	Al	0.17	Al	0.04
C	2.00	F	2.47					Mg	0.88	Mg	0.04
		OH	0.53					Mn	0.11	Mn	0.01
										Ca	0.01

*Calculated from stoichiometry; **calculated for a sum (F+OH) = 3 apfu; FeO_t = all Fe as total iron; [§]Fe_2O_3 and FeO calculated according to Droop (1987).

TABLE 4. Whole-rock major element oxides (wt%) and trace element (ppm) compositions of selected Fiano xenoliths.

Sample ID	TF1	TF2	TF4	TF5	TF6	TF9	TF12	TF8	TF11	TF15
			Micaceous xenoliths					*Carbonate xenoliths*		
SiO_2	25.33	20.44	13.51	14.00	13.06	14.04	14.76	7.10.	5.55	7.33
Al_2O_3	3.59	3.05	2.47	3.06	2.90	4.12	2.75	1.00	1.01	1.50
Fe_2O_3	2.00	1.04	1.19	1.65	1.22	1.00	2.05	0.70	0.52	0.66
MnO	0.32	0.33	0.21	0.24	0.23	0.26	0.70	0.22	0.76	0.25
MgO	29.00	18.54	19.45	22.00	21.13	20.55	18.11	9.88	6.66	9.00
CaO	17.88	30.97	39.11	36.68	39.15	38.95	39.15	41.30	44.53	41.01
Na_2O	1.33	0.55	0.29	0.34	0.30	0.26	0.99	0.07	0.50	0.03
K_2O	2.94	3.00	2.39	2.55	2.05	2.60	2.66	0.60	0.54	0.03
TiO_2	0.11	0.18	0.06	0.09	0.07	0.05	1.70	0.04	0.03	0.01
P_2O_5	0.04	0.30	0.01	0.60	0.01	0.03	0.03	0.01	0.07	0.02
LOI	16.73	20.66	20.65	17.11	19.00	17.00	16.90	38.99	40.00	39.43
Total	99.27	99.06	99.34	98.32	99.12	98.86	99.80	99.95	100.17	99.27
Be	4.2	5.0	8.0	7.7	8.1	6.7	4.9	2.0	3.0	3.0
B	8991	4567	7421	8965	8065	8991	6993	100	98	102
Sc	2	1	–	1.0	–	–	1.0	–	–	–
V	53	44	49	47	51	52	48	30	57	33
Cr	23	27	20	22	23	24	24	12	19	13
Co	4	3.3	2.8	2.9	3	2.3	4	0.5	3	0.5
Ni	0.9	0.6	0.5	0.6	0.49	0.61	0.52	11	9	12
Cu	7.6	8	8.1	7.65	7.9	7.1	6.95	8	7	9
Zn	373.1	334	304	299	293	279	307	156	163	154
Ga	5	5.2	4.4	4	5	5	4.8	4	5.5	3
As	2788	2800	2502.2	3007	2574	2812	2500	12	150	16
Se	2	1.1	1	2	1.3	1.5	2	0.5	2	0.4
Rb	431	447	401.6	500	408	399	411	59	104	50
Sr	112	132	103.4	96	100	100	99	399	170	200
Y	4.2	4	3.9	5	4.4	4	4.7	1	7	2
Zr	29	31	34.4	25	28	27	29	8	17	9
Nb	15.3	14	14.1	14	15	14.1	14.5	4	9	5
Mo	2.4	2	1.5	3	2	3.2	2	6	5	5
Ag	0.7	0.7	0.5	1	1	1.1	1.2	0.4	1	0.45
Cd	0.12	0.09	0.05	0.06	0.10	0.1	0.11	0.2	0.1	0.22
Sn	32	26	29	33	30	30	33	2.3	19	2.4
Sb	6	6.3	7.2	7	6	8	7	1	5	2
Cs	57	59	65.7	59	58	60	62	3	20	4
Ba	18	18.1	17	16	16.8	16.4	17	26	20	28
La	5.7	5.99	6	5.73	6.11	5.44	5.7	3.7	4.5	3.9
Ce	10.7	10.6	10.8	10.6	10.5	10	10.54	7.85	8.9	8
Pr	1.1	1.21	1.22	1.1	1.16	1.03	1.04	0.71	0.96	0.8
Nd	4	4.2	4.4	4	3.9	3.8	3.91	2.1	2.9	2.5
Sm	0.6	0.62	0.62	0.6	0.63	0.59	0.56	0.4	0.45	0.41
Eu	0.1	0.1	0.08	0.09	0.08	0.09	0.082	0.06	0.069	0.057
Gd	0.51	0.5	0.57	0.44	0.52	0.49	0.52	0.39	0.43	0.35
Tb	0.08	0.079	0.09	0.082	0.087	0.085	0.087	0.06	0.063	0.055
Dy	0.45	0.46	0.56	0.49	0.5	0.5	0.53	0.33	0.36	0.358
Ho	0.09	0.092	0.11	0.096	0.099	0.095	0.1	0.07	0.077	0.071
Er	0.25	0.27	0.33	0.29	0.285	0.3	0.3	0.19	0.22	0.2
Tm	0.033	0.037	0.04	0.038	0.039	0.04	0.039	0.027	0.03	0.029
Yb	0.24	0.26	0.32	0.289	0.299	0.3	0.25	0.17	0.2	0.186
Lu	0.037	0.039	0.05	0.044	0.045	0.046	0.038	0.027	0.031	0.029
Hf	0.8	0.66	0.6	0.7	0.71	0.65	0.73	0.02	0.68	0.03
Ta	0.9	0.76	0.6	0.72	0.66	0.7	0.68	0.05	0.36	0.05
W	8	7.99	8.9	9	8.5	9.1	8.8	0.6	8	0.7
Au*	15	14	14.4	13.9	14.3	13.6	14	5	8	6.1
Hg	0.6	0.5	0.33	0.32	0.35	0.33	0.33	0.2	0.3	0.3
Tl	0.2	0.2	0.3	0.2	0.22	0.22	0.19	0.1	0.2	0.11
Pb	76	79	77.9	81	79	80	75	200	76	203
Bi	0.7	0.5	0.5	0.7	0.6	0.65	0.6	2.9	0.55	2.6
Th	1.3	1.37	1.4	1.45	1.45	1.7	1.3	0.7	1.6	0.8
U	6	5.7	5.5	5	6	5.3	5.1	0.8	2.5	0.9

– not detcetd. *ppb

This is a 'preproof' accepted article for Mineralogical Magazine.
This version may be subject to change during the production process.
10.1180/minmag.2016.080.155

TABLE 5. Oxygen and carbon isotope compositions of calcite from selected Fiano xenoliths.

Sample ID	$\delta^{13}C$ (‰ VPDB)	$\delta^{18}O$ (‰ VPDB)	$\delta^{18}O$ (‰ VSMOW)
Micaceous xenoliths			
TF5	-4.28	-14.72	15.68
TF6	-5.20	-9.43	21.13
TF9	-1.61	-11.15	19.37
TF13	-0.64	-7.13	23.51
Carbonate xenoliths			
TF8	-1.60	-3.62	27.12
TF11	-4.31	-10.47	20.06
TF14	-0.07	-4.28	26.45
TF15	-3.89	-11.01	19.51
TF16	0.04	-6.12	24.56

TABLE 6. Electron microprobe analyses (wt.%) and atomic ratios (a.p.f.u.) calculated on the basis of 12(O, OH, F) of the studied micas.

	TF2_1	TF2_2	TF7_1	TF7_2	TF10_1	TF10_2
SiO_2	43.6(2)	44.0(2)	43.7(3)	43.7(3)	44.2(2)	43.2(2)
Al_2O_3	11.0(1)	12(1)	10.8(5)	10.8(2)	11.1(5)	10.8(6)
MgO	26.3(3)	25.9(2)	28.1(7)	28.0(2)	27.9(4)	27.2(2)
FeO_t[a]	3.1(1)	2.9(2)	2.0(3)	1.5(2)	1.5(2)	1.6(1)
TiO_2	0.10(3)	0.08(2)	0.06(3)	0.09(3)	0.13(5)	0.09(3)
MnO	0.26(4)	0.21(4)	0.14(3)	0.19(4)	0.25(6)	0.33(1)
ZnO	b.d.l.	b.d.l.	b.d.l.	0.13(9)	b.d.l.	b.d.l.
K_2O	9.38(7)	9.17(8)	9.62(8)	9.67(4)	9.69(4)	9.12(6)
Na_2O	0.76(2)	0.91(1)	0.57(4)	0.65(4)	0.57(4)	0.79(2)
CaO	b.d.l.	b.d.l.	0.06(6)	0.10(6)	b.d.l.	b.d.l.
F	8.0(2)	8.9(1)	9.1(2)	9.1(1)	8.9(1)	8.9(5)
Cl	b.d.l.	0.08(3)	b.d.l.	b.d.l.	b.d.l.	b.d.l.
Total	102.5(3)	104(1)	104.2(7)	103.9(2)	104.2(8)	102(1)
O=F, Cl	-3.39	-3.78	-3.82	-3.84	-3.76	-3.75
	99.11	100.22	100.38	100.06	100.44	98.25
Si	3.06	3.06	3.05	3.05	3.06	3.06
Al^{IV}	0.85	0.93	0.88	0.87	0.91	0.91
Fe^{IV}	0.09	0.00	0.06	0.08	0.03	0.03
sum	4.00	3.99	3.99	4.00	4.00	4.00
Al^{VI}	0.05	0.03	0.00	0.02	0.00	0.00
Mg	2.75	2.69	2.91	2.92	2.89	2.88
Fe_t^{VI}	0.09	0.17	0.05	0.01	0.05	0.06
Ti	0.01	0.00	0.00	0.00	0.01	0.00
Mn	0.02	0.01	0.01	0.01	0.01	0.02
Zn	0.00	0.00	0.00	0.01	0.00	0.00
sum	2.92	2.92	2.97	2.97	2.96	2.96
K	0.84	0.81	0.86	0.86	0.86	0.82
Na	0.10	0.12	0.08	0.09	0.08	0.11
Ca	0.00	0.00	0.00	0.01	0.00	0.00
sum	0.94	0.94	0.94	0.96	0.94	0.93

[a] FeOt is total iron. bdl = below detection limit.

TABLE 7. Crystallographic data of the studied micas.

	TF2_1	TF2_2	TF7_1	TF7_2	TF10_1	TF10_2
Crystal size $(mm)^3$	0.35x0.15 x0.01	0.38x0.19 x0.03	0.45x0.25 x0.02	0.46x0.39 x0.06	0.48x0.47 x0.04	0.65x0.47 x0.02
Space group	*C2/m*	*C2/m*	*C2/m*	*C2/m*	*C2/m*	*C2/m*
a (Å)	5.3030(1)	5.3002(1)	5.3044(3)	5.3056(1)	5.3047(1)	5.3083(1)
b (Å)	9.1866(2)	9.1830(2)	9.1891(4)	9.1925(2)	9.1882(2)	9.1919(3)
c (Å)	10.1298(2)	10.1298(2)	10.1360(6)	10.1288(3)	10.1298(2)	10.1291(3)
β (°)	100.074(2)	100.046(1)	100.109(4)	100.077(2)	100.071(1)	100.093(2)
Cell volume $(Å^3)$	485.88(2)	485.48(2)	486.39(5)	486.38(2)	486.13(2)	486.58(2)
Z	4	4	4	4	4	4
Reflections collected	4955	4985	3876	6027	6405	5980
Reflections unique	1239	1241	1241	1768	1745	1785
$R_{merging}$ [$R_{(int)}$] (%)	3.13	2.23	4.11	1.65	1.85	2.16
Reflections used ($I>3\sigma(I)$)	950	1041	834	1495	1430	1330
No. of refined parameters	63	63	61	61	61	61
Goof[a]	1.110	1.051	1.062	1.045	1.041	1.101
R_1[b] (%)	2.68	1.99	4.37	1.78	1.92	2.48
wR_2[c] (%)	2.50	2.82	5.10	2.21	2.28	2.71
$\Delta\rho_{min}/\Delta\rho_{max}$ $(e^-/Å^3)$	-0.41/0.53	-0.23/0.61	-0.81/0.57	-0.21/0.41	-0.33/0.43	-0.37/0.65

a: Goodness-of-fit = $[\Sigma[w(F_o^2-F_c^2)^2]/(N\text{-p})]^{1/2}$, where *N* and *p* are the number of reflections and parameters. respectively.
b: $R_1 = \Sigma[|F_o| - |F_c|]/\Sigma|F_o|$.
c: $wR_2 = [\Sigma[w(F_o-F_c)^2]/\Sigma[w(F_o)^2]]^{1/2}$; *w* = Chebyshev optimized weights.

This is a 'preproof' accepted article for Mineralogical Magazine.
This version may be subject to change during the production process.
10.1180/minmag.2016.080.155

TABLE 8. Structural formulas in atoms per formula unit (a.p.f.u.) of the studied micas.

	Interlayer	Octahedral site	Tetrahedral site	Anionic site
TF2_1	$(K_{0.84}Na_{0.10})_{\Sigma=0.94}$	$(Mg_{2.75}Mn_{0.02}Fe^{3+}_{0.09}Al_{0.05}Ti_{0.01}[]_{0.08})_{\Sigma=3.00}$	$(Si_{3.06}Al_{0.85}Fe^{3+}_{0.09})_{\Sigma=4.00}$	$O_{10.01}OH_{0.21}F_{1.78}$
TF2_2	$(K_{0.81}Na_{0.12})_{\Sigma=0.93}$	$(Mg_{2.69}Mn_{0.01}Fe^{3+}_{0.17}Al_{0.02}[]_{0.11})_{\Sigma=3.00}$	$(Si_{3.06}Al_{0.94})_{\Sigma=4.00}$	$O_{10.00}OH_{0.03}Cl_{0.01}F_{1.96}$
TF7_1	$(K_{0.86}Na_{0.08})_{\Sigma=0.94}$	$(Mg_{2.91}Mn_{0.01}Fe^{3+}_{0.04}[]_{0.04})_{\Sigma=3.00}$	$(Si_{3.05}Al_{0.88}Fe^{3+}_{0.07})_{\Sigma=4.00}$	$O_{10.00}F_{2.00}$
TF7_2	$(K_{0.86}Na_{0.08}\ Ca_{0.01})_{\Sigma=0.96}$	$(Mg_{2.92}Mn_{0.01}Zn_{0.01}Fe^{3+}_{0.01}Al_{0.02}[]_{0.02})_{\Sigma=2.98}$	$(Si_{3.05}Al_{0.87}Fe^{3+}_{0.08})_{\Sigma=4.00}$	$O_{10.00}F_{2.01}$
TF10_1	$(K_{0.86}Na_{0.08})_{\Sigma=0.93}$	$(Mg_{2.89}Mn_{0.01}Fe^{3+}_{0.05}Ti_{0.01}[]_{0.04})_{\Sigma=3.00}$	$(Si_{3.06}Al_{0.91}Fe^{3+}_{0.03})_{\Sigma=4.00}$	$O_{10.00}OH_{0.04}F_{1.96}$
TF10_2	$(K_{0.82}Na_{0.11})_{\Sigma=0.93}$	$(Mg_{2.88}Mn_{0.02}Fe^{3+}_{0.06}[]_{0.03})_{\Sigma=2.99}$	$(Si_{3.06}Al_{0.91}Fe^{3+}_{0.03})_{\Sigma=4.00}$	$O_{10.00}F_{2.00}$

SUPPLEMENTARY TABLE S1. Crystallographic coordinates, occupancies, equivalent isotropic ($Å^2$) and anisotropic displacement parameters of the studied micas.

Sample TF2_1

Site	Atom	*x*/*a*	*y*/*b*	*z*/*c*	Occupancy	$U_{iso/equiv}$	U_{11}	U_{22}	U_{33}	U_{23}	U_{13}	U_{12}
K	K^+	0	½	0	0.937(1)	0.0287	0.0291(4)	0.0296(4)	0.0272(3)	0	0.0044(3)	0
M1	Mg^{2+} Fe^{2+}	0	0	½	0.971(2) 0.029(1)	0.0097	0.0084(4)	0.0077(4)	0.0136(4)	0	0.0031(2)	0
M2	Mg^{2+} Fe^{2+}	0	0.33174(6)	½	0.975(2) 0.025(2)	0.0095	0.0074(2)	0.0085(3)	0.0125(3)	0	0.00157(16)	0
T	Si, Si^{4+}	0.07514(6)	0.16663(3)	0.22481(3)	1.003(7)	0.0092	0.0080(1)	0.0086(1)	0.0111(1)	-0.0002(1)	0.00181(8)	-0.0002(1)
O1	O, O^{2-}	0.3209(2)	0.2344(1)	0.16603(9)	1.000(7)	0.0180	0.0165(4)	0.0230(5)	0.0148(4)	-0.0013(3)	0.0033(3)	-0.0059(3)
O2	O, O^{2-}	0.0245(3)	0	0.1661(1)	1.000(7)	0.0180	0.0247(6)	0.0142(6)	0.0139(5)	0	0.0004(5)	0
O3	O, O^{2-}	0.1305(1)	0.16657(9)	0.39020(8)	1.000(7)	0.0092	0.0085(3)	0.0089(3)	0.0103(3)	-0.0003(3)	0.0020(2)	0.0000(3)
O4	F^-	0.1333(2)	0.5	0.4016(1)	1.000	0.0120	0.0102(4)	0.0124(4)	0.0134(4)	0	0.0017(3)	0

Sample TF2_2

Site	Atom	*x*/*a*	*y*/*b*	*z*/*c*	Occupancy	$U_{iso/equiv}$	U_{11}	U_{22}	U_{33}	U_{23}	U_{13}	U_{12}
K	K^+	0	½	0	0.927(1)	0.0287	0.0288(2)	0.0303(3)	0.0269(2)	0	0.0047(2)	0
M1	Mg^{2+} Fe^{2+}	0	0	½	0.984(2) 0.016(1)	0.0093	0.0080(3)	0.0073(3)	0.0131(3)	0	0.0032(2)	0
M2	Mg^{2+} Fe^{2+}	0	0.33195(4)	½	0.981(2) 0.019(2)	0.0093	0.0069(2)	0.0084(2)	0.0127(2)	0	0.0019(1)	0
T	Si, Si^{4+}	0.07506(4)	0.16663(2)	0.22492(2)	1.001(7)	0.0091	0.0081(1)	0.0087(1)	0.0108(1)	-0.00019(6)	0.00204(6)	-0.00009(5)
O1	O, O^{2-}	0.3205(1)	0.23484(8)	0.16606(6)	1.000(7)	0.0181	0.0164(2)	0.0234(3)	0.0148(2)	-0.0015(2)	0.0033(2)	-0.0064(2)
O2	O, O^{2-}	0.0249(2)	0	0.16604(9)	1.000(7)	0.0182	0.0251(4)	0.0134(3)	0.0154(3)	0	0.0016(3)	0
O3	O, O^{2-}	0.1302(1)	0.16662(5)	0.39024(6)	1.000(7)	0.0093	0.0087(2)	0.0089(2)	0.0104(2)	-0.0004(1)	0.0020(2)	-0.0001(1)
O4	F^-	0.1335(1)	0.5	0.40160(7)	1.000	0.0118	0.0099(2)	0.0116(3)	0.0137(3)	0	0.0020(2)	0

This is a 'preproof' accepted article for Mineralogical Magazine.
This version may be subject to change during the production process.
10.1180/minmag.2016.080.155

Sample TF7_1

Site	Atom	*x*/*a*	*y*/*b*	*z*/*c*	Occupancy	$U_{iso/equiv}$	U_{11}	U_{22}	U_{33}	U_{23}	U_{13}	U_{12}
K	K^{+}	0	½	0	0.9352(18)	0.0330	0.0329(7)	0.0346(7)	0.0321(7)		0 0.0069(5)	0
M1	Mg^{2+}	0	0	½	1.0014(9)	0.0133	0.0099(5)	0.0110(6)	0.0197(7)		0 0.0044(5)	0
M2	Mg^{2+}	0	0.3317(1)	½	1.0010(9)	0.0130	0.0090(4)	0.0113(4)	0.0189(5)		0 0.0030(3)	0
T	Si. Si^{4+}	0.0748(1)	0.16663(6)	0.22508(6)	1.000(7)	0.0123	0.0102(2)	0.0118(2)	0.0156(2)	-0.0003(2)	0.0038(2)	-0.0003(2)
O1	O, O^{2-}	0.3208(3)	0.2342(2)	0.1659(2)	1.000(7)	0.0210	0.0173(6)	0.0259(8)	0.0206(7)	-0.0014(6)	0.0054(6)	-0.0057(6)
O2	O, O^{2-}	0.0230(5)	0	0.1659(3)	1.000(7)	0.0222	0.026(1)	0.018(1)	0.021(1)		0 0.0023(9)	0
O3	O, O^{2-}	0.1301(3)	0.1666(2)	0.3907(2)	1.000(7)	0.0122	0.0089(5)	0.0111(5)	0.0173(6)	-0.0001(5)	0.0041(4)	0.0005(4)
O4	F^{-}	0.1336(3)	0.5	0.4021(2)	1.000	0.0140	0.0099(6)	0.0148(7)	0.0180(8)		0 0.0044(6)	0

Sample TF7_2

Site	Atom	*x*/*a*	*y*/*b*	*z*/*c*	Occupancy	$U_{iso/equiv}$	U_{11}	U_{22}	U_{33}	U_{23}	U_{13}	U_{12}
K	K^{+}	0	½	0	0.9292(7)	0.0287	0.0301(3)	0.0302(2)	0.0258(2)	0	0.0050(1)	0
M1	Mg^{2+}	0	0	½	0.9939(6)	0.0090	0.0079(1)	0.0074(1)	0.0120(2)	0	0.0024(1)	0
M2	Mg^{2+}	0	0.33144(3)	½	0.9968(8)	0.0090	0.00776(9)	0.00741(9)	0.0119(1)	0	0.00232(7)	0
T	Si, Si^{4+}	0.07505(3)	0.16663(1)	0.22480(1)	1.005(7)	0.0089	0.00869(5)	0.00823(5)	0.00992(6)	-0.00002(4)	0.00210(4)	-0.00001(3)
O1	O, O^{2-}	0.32166(9)	0.23382(5)	0.16621(4)	1.000(7)	0.0182	0.0172(2)	0.0237(2)	0.0141(2)	-0.0016(1)	0.0037(1)	-0.0063(1)
O2	O, O^{2-}	0.0233(1)	0	0.16628(6)	1.000(7)	0.0182	0.0263(3)	0.0135(2)	0.0141(2)	0	0.0012(2)	0
O3	O, O^{2-}	0.13022(6)	0.16656(3)	0.39036(4)	1.000(7)	0.0088	0.0089(1)	0.0081(1)	0.0096(1)	-0.00009(8)	0.00203(9)	0.00012(8)
O4	F^{-}	0.13323(8)	0.5	0.40212(5)	1.000	0.0107	0.0099(1)	0.0102(1)	0.0119(2)	0	0.0020(1)	0

Sample TF10_1

Site	Atom	*x*/*a*	*y*/*b*	*z*/*c*	Occupancy	$U_{iso/equiv}$	U_{11}	U_{22}	U_{33}	U_{23}	U_{13}	U_{12}
K	K^{+}	0	½	0	0.9289(7)	0.0279	0.0289(2)	0.0292(2)	0.0256(2)		0 0.0044(1)	0
M1	Mg^{2+}	0	0	½	0.9931(6)	0.0084	0.0067(2)	0.0066(2)	0.0120(2)		0 0.0022(1)	0
M2	Mg^{2+}	0	0. 33163(3)	½	0.9996(8)	0.0084	0.0065(1)	0.0070(1)	0.0117(1)		0 0.00195(8)	0
T	Si, Si^{4+}	0.07515(3)	0.16662(2)	0.22488(2)	1.004(7)	0.0082	0.00737(6)	0.00746(6)	0.00978(7)	-0.00005(4)	0.00180(4)	0.00000(4)
O1	O, O^{2-}	0.3213(1)	0.23430(6)	0.16616(5)	1.000(7)	0.0173	0.0153(2)	0.0230(2)	0.0139(2)	-0.0014(2)	0.0032(1)	-0.0063(2)
O2	O, O^{2-}	0.0240(2)	0	0.16609(7)	1.000(7)	0.0173	0.0256(3)	0.0118(2)	0.0135(3)		0 0.0009(2)	0
O3	O, O^{2-}	0.13026(7)	0.16653(4)	0.39034(4)	1.000(7)	0.0081	0.00740(1)	0.0080(1)	0.0091(2)	-0.0001(1)	0.0017(1)	0.00013(9)
O4	F^{-}	0.13342(9)	0.5	0.40208(5)	1.000	0.0101	0.0090(2)	0.0094(2)	0.0180(2)		0 0.0018(1)	0

Sample TF10_2

Site	Atom	*x*/*a*	*y*/*b*	*z*/*c*	Occupancy	$U_{iso/equiv}$	U_{11}	U_{22}	U_{33}	U_{23}	U_{13}	U_{12}
K	K^{+}	0	½	0	0.9339(8)	0.0308	0.0311(3)	0.0313(3)	0.0301(3)	0	0.0058(2)	0
M1	Mg^{2+}	0	0	½	0.9956(7)	0.0107	0.0089(2)	0.0081(2)	0.0156(2)	0	0.0034(2)	0
M2	Mg^{2+}	0	0. 33159(4)	½	0.9986(8)	0.0105	0.0085(1)	0.0084(2)	0.0149(2)	0	0.0028(1)	0
T	Si, Si^{4+}	0.07511(4)	0.16664(2)	0.22480(2)	1.003(7)	0.0106	0.00948(9)	0.00909(8)	0.01352(9)	-0.00001(7)	0.00287(6)	-0.00003(6)
O1	O, O^{2-}	0.3215(1)	0.23400(9)	0.16615(7)	1.000(7)	0.0200	0.0185(3)	0.0245(3)	0.0178(3)	-0.0013(2)	0.0049(2)	-0.0064(2)
O2	O, O^{2-}	0.0234(2)	0	0.1662(1)	1.000(7)	0.0200	0.0275(5)	0.0147(3)	0.0173(4)	0	0.0020(3)	0
O3	O, O^{2-}	0.1302(1)	0.16647(6)	0.39041(6)	1.000(7)	0.0105	0.0095(2)	0.0090(2)	0.0131(2)	-0.0003(2)	0.0027(2)	0.0000(1)
O4	F^{-}	0.1333 (1)	0.5	0.40210(7)	1.000	0.0123	0.0107(2)	0.0109(2)	0.0156(3)	0	0.0029(2)	0

SUPPLEMENTARY TABLE S2. Selected bond distances (Å) of the studied micas.

	TF2_1	TF2_2	TF7_1	TF7_2	TF10_1	TF10_2
T-O1	1.647(1)	1.646(1)	1.650(2)	1.648(1)	1.648(1)	1.649(1)
T-O1'	1.649(1)	1.647(1)	1.650(2)	1.648(1)	1.648(1)	1.649(1)
T-O2	1.647(1)	1.647(0)	1.650(1)	1.648(0)	1.648(0)	1.648(0)
T-O3	1.650(1)	1.649(1)	1.653(2)	1.651(0)	1.650(0)	1.652(1)
<T-O>	1.648(1)	1.647(1)	1.651(2)	1.649(0)	1.649(0)	1.650(1)
M1-O4(x2)	2.024(1)	2.023(1)	2.021(2)	2.024(0)	2.023(1)	2.024(1)
M1-O3(x4)	2.080(1)	2.079(1)	2.077(1)	2.079(0)	2.079(0)	2.079(1)
<M1-O>	2.061(1)	2.060(1)	2.058(1)	2.061(0)	2.060(0)	2.060(1)
M2-O4(x2)	2.032(1)	2.030(1)	2.031(1)	2.032(0)	2.031(0)	2.031(1)
M2-O3(x2)	2.071(1)	2.070(1)	2.067(2)	2.068(0)	2.069(0)	2.069(1)
M2-O3'(x2)	2.077(1)	2.078(1)	2.077(1)	2.079(0)	2.078(0)	2.079(1)
<M2-O>	2.060(1)	2.059(5)	2.058(1)	2.059(0)	2.059(0)	2.060(1)
<M-O>	2.060(1)	2.060(1)	2.058(1)	2.060(1)	2.060(0)	2.060(1)
K-O1(x4)	2.988(1)	2.991(1)	2.987(2)	2.984(1)	2.988(1)	2.986(1)
K-O1'(x4)	3.267(1)	3.263(1)	3.269(2)	3.275(1)	3.270(1)	3.274(1)
K-O2 (x2)	2.988(1)	2.990(1)	2.981(3)	2.985(1)	2.987(1)	2.986(1)
K-O2'(x2)	3.267(1)	3.263(1)	3.275(3)	3.275(1)	3.270(1)	3.275(1)
$<K\text{-}O>_{inner}$	2.988(1)	2.991(1)	2.984(2)	2.985(1)	2.987(1)	2.986(1)
$<K\text{-}O>_{outer}$	3.267(1)	3.263(1)	3.271(2)	3.275(1)	3.270(1)	3.274(1)
<K-O>	3.128(1)	3.127(1)	3.127(2)	3.130(1)	3.128(1)	3.130(1)

This is a 'preproof' accepted article for Mineralogical Magazine.
This version may be subject to change during the production process.
10.1180/minmag.2016.080.155

SUPPLEMENTARY TABLE S3. Distortional parameters (calculated as indicated in Lacalamita *et al.*, 2011) for the studied micas. Errors on distortion parameters, estimated by varying the refined positional parameters within one standard deviation are in the following ranges: < 0.5% for volumes, thicknesses, projected bond lengths, shifts; 0.1-13% for angles, bond/edge lengths distortions, sheet corrugations, D.M., $\Delta_{K\text{-}O}$.

	TF2_1	TF2_2	TF7_1	TF7_2	TF10_1	TF10_2
t_{tet} [Å]	2.236	2.236	2.243	2.235	2.236	2.236
BLDT	0.063	0.047	0.063	0.067	0.050	0.063
$Volume_T$ [Å3]	2.295	2.293	2.305	2.300	2.298	2.301
TQE	1.0006	1.0006	1.0007	1.0007	1.0006	1.0005
TAV[°]	2.49	2.67	2.98	2.95	2.45	2.28
τ [°]	110.8	110.9	111.0	110.7	110.8	110.8
α[°]	6.17	6.00	6.25	6.40	6.21	6.32
Δz [Å]	0.0007	0.0002	0.0000	0.0007	0.0007	0.0005
D.M. [Å]	0.497	0.494	0.510	0.510	0.505	0.510
$\psi_{M(1)}$ [°]	59.15	59.13	59.24	59.23	59.20	59.23
$\psi_{M(2)}$ [°]	59.12	59.12	59.24	59.20	59.19	59.22
$BLD_{M(1)}$	1.213	1.209	1.215	1.203	1.212	1.180
$ELD_{M(2)}$	5.297	5.278	5.412	5.392	5.365	5.396
$BLD_{M(1)}$	0.901	0.945	1.215	1.272	1.270	1.275
$ELD_{M(2)}$	5.261	5.257	5.401	5.361	5.344	5.380
$Shift_{M(2)}$ [Å]	0.0016	0.0014	0.0016	0.0019	0.00017	0.00017
$Volume_{M(1)}$ [Å]	11.460	11.441	11.406	11.441	11.432	11.434
$OQE_{M(1)}$	1.013	1.013	1.013	1.013	1.013	1.013
$OAV_{M(1)}$[°]	41.21	40.79	42.84	42.65	42.26	42.75
$Volume_{M(2)}$ [Å3]	11.438	11.429	11.402	11.420	11.419	11.426
$OQE_{M(2)}$	1.013	1.013	1.013	1.013	1.013	1.013
$OAV_{M(2)}$[°]	41.46	41.35	43.25	42.76	42.47	43.02
$eu_{M(1)}/es_{M(1)}$	1.112	1.111	1.114	1.114	1.113	1.114
$eu_{M(2)}/es_{M(2)}$	1.111	1.111	1.114	1.113	1.113	1.113
t_{oct} [Å]	2.114	2.114	2.105	2.109	2.109	2.108
t_{int} [Å]	3.312	3.313	3.311	3.316	3.314	3.314
ΔK-O [Å]	0.279	0.272	0.285	0.290	0.284	0.288
$t_{K\text{-}O4}$ [Å]	3.944	3.944	3.950	3.948	3.948	3.948

SUPPLEMENTARY TABLE S4. Mean distances (Å) and mean atomic numbers (electrons, e^-) of cation sites derived by structure refinements (X-ref) and chemical analyses (EMP). Average error for mean atomic numbers is ± 0.5 e^-.

	TF2_1	TF2_2	TF7_1	TF7_2	TF10_1	TF10_2
e^- (M1) X-ref	12.41	12.22	12.02	11.93	11.92	11.95
e^- (M2) X-ref	12.35	12.27	12.01	11.96	12.00	11.98
e^- (M1+2M2) X-ref	37.11	36.76	36.04	35.85	35.92	35.91
e^- (M1+2M2) EMP	36.71	36.21	36.21	36.11	36.45	36.62
K e^- X-ref	17.80	17.61	17.77	17.65	17.65	17.74
K e^- EMP	17.06	16.71	17.22	17.53	17.22	16.79
T e^- X-ref	14.04	14.01	14.00	14.07	14.06	14.04
T e^- EMP	14.06	13.86	14.19	14.02	13.86	13.86
<M-O> X-ref	2.060	2.060	2.058	2.060	2.060	2.060
<M-O> EMP	2.070	2.067	2.073	2.070	2.072	2.070
<T-O> X-ref	1.648	1.647	1.651	1.649	1.649	1.650
<T-O> EMP	1.653	1.650	1.651	1.653	1.651	1.651

This is a 'preproof' accepted article for Mineralogical Magazine.
This version may be subject to change during the production process.
10.1180/minmag.2016.080.155